Implications of Hf isotopes for the evolution of the mantle source of magmas associated with the giant El Teniente Cu-Mo megabreccia deposit, central Chile

Charles R. Stern[1,*], Kwan-Nang Pang[2], Hao-Yang Lee[2], M. Alexandra Skewes[1], Alejandra Arévalo[3]

[1] Department of Geological Sciences, University of Colorado, Boulder, Colorado, 80309-0399 USA; Charles.Stern@colorado.edu

[2] Institute of Earth Sciences, Academia Sinica, Taipei, Taiwan; knpang@earth.sinica.edu.tw

[3] Escuela de Ingeniería, Universidad de O'Higgins, VI Región, Chile; aarevalot@gmail.com

* Correspondence: Charles.Stern@colorado.edu; Tel. +1-303-492-7170

Abstract: We have determined the Hf isotopic compositions of 12 samples associated with the giant El Teniente Cu-Mo megabreccia deposit, central Chile. The samples range in age from ≥8.9 to 2.3 Ma and provide information about the temporal evolution of their magmatic sources from the Late Miocene to Pliocene. Together with previously published data, the new analysis indicate a temporal decrease of 10 $\varepsilon_{Hf(t)}$ units, from +11.6 down to +1.6, in the 12.7 m.y. from 15 to 2.3 Ma. These variations imply increasing incorporation of continental crust through time in the magmas that formed these rocks. The fact that the samples include mantle-derived olivine basalts and olivine lamprophyres suggests that these continental components were incorporated into their mantle source, and not by intra-crustal contamination (MASH). We attribute the increase, between the Middle Miocene and Pliocene, of crustal components in the subarc mantle source below El Teniente to be due to increased rates of subduction erosion and transport of crust into the mantle. The deposit formed above a large, long-lived, vertically zoned magma chamber that developed due to compressive deformation and persisted between ~7 to 4.6 Ma. Progressively more hydrous mantle-derived mafic magmas feed this chamber from below, providing heat, H_2O, S and metals, but no unique "fertile" Cu-rich magma was involved in the formation of the deposit. As the volume of these mantle-derived magmas decreased from the Late Miocene into the Pliocene, the chamber crystallized and solidified, producing felsic plutons and large metal-rich magmatic-hydrothermal breccias that emplaced Cu and S into the older (≥8.9 Ma) mafic host rocks of this megabreccia deposit.

Keywords: El Teniente Cu-Mo deposit, Andean magmatism, subduction erosion, mantle source region contamination, Hafnium isotopes

1. Introduction

The isotopic compositions ($^{87}Sr/^{86}Sr$ ≥0.7050; ε_{Nd} ≤-2; $\varepsilon_{Hf(t)}$ ≤+2) of some recently erupted Andean volcanic rocks indicate that they have incorporated continental crust [1-5]. Two different processes for the incorporation of crust into Andean magmas have been proposed (Figure 1). One, MASH (Mixing, Assimilation, Storage and Homogenization), involves intra-crustal assimilation as mantle-derived magmas rise from their source through the crust to the surface [2]. Another, PEELED, involves a mantle source region contaminated by crustal components subducted below the mantle wedge and then released into the wedge by either melting or dehydration and volatile transport [3,4]. These two different models have very different implications for geochemical cycling associated with subduction zones, and for the growth and evolution of both the continental crust and mantle [5].
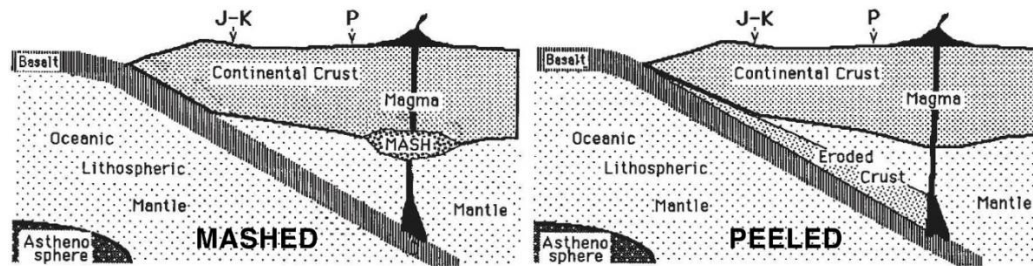
Figure 1. Two alternative explanations, as originally illustrated by Hickey-Vargas in 1991 [1], for the incorporation of continental crust into Andean magmas. MASHED on the left involves Mixing, Assimilation, Storage and Homogenization in a MASH zone located at either the lower crust/mantle boundary or within the crust [2]. PEELED on the right involves recycling of subduction eroded crust into the mantle wedge source [3-5]. J-K and P indicate the positon of the Jurassic-Cretaceous and Pliocene plutonic belts, respectively, in the Andes of northern Chile. The recently active volcanic arc is ~250 km east of the Jurassic arc as a result in part of subduction erosion [6]. (Reprinted from Nature, volume 350, R. Hickey-Vargas, Peeled or MASHed?, page 350, Copyright 1991, with permission from Springer Nature.)

The amount of crustal components incorporated into recently erupted Andean volcanic rocks varies along strike from south-to-north, as do various geologic and tectonic features such as crustal thickness and age, subduction angle, trench depth and sediment fill, and the localized presence of bouyant features such as oceanic seamount chains and spreading ridges being subducted below the South American continental margin (Figure 2; [4]). For instance, in the Central Volcanic Zone (CVZ) of northern Chile, the crust is much thicker (≥70 km) than below the central part of the Southern Volcanic Zone (≤35 km; CSVZ; Figure 2) and the isotopic compositions of the recently erupted volcanic rocks suggests more crustal components have been incorporated in CVZ than CSVZ magmas [3-5]. This could reflect greater amounts of crustal assimilation by mantle-derived magmas as they rose through the thicker CVZ crust, but in this same region the trench is devoid of sediment due to the arid conditions in northern Chile, and compared to the CSVZ, much more significant amounts of subduction erosion, at rates estimated to be 50–70 km^3/km/my since ~150 Ma (Figure 2; [5]), have truncated the continental margin [6] and caused the arc to migrate eastward ~250 km since the Jurassic (Figure 1). The subduction of tectonically eroded crust has been invoked not only to explain the crustal components in CVZ magmas [3-5,7,8], but also the uplift and crustal thickening observed in this part of the Andes [9].

In the same way, at the northern end of the Andean SVZ (NSVZ; Figures 2 and 3), where the MASH model was first presented [2], the crust thickens to ≥60 km compared to ≤35 km below the CSVZ, and the isotopic compositions of recently erupted volcanic rocks indicate that they contain greater amount of crustal components [3-5,10,11]. However, the subduction of the Juan Fernández Ridge has caused the subduction angle to flatten, increasing the rate of subduction erosion west of the NSVZ to between 115 to 230 km^3/km/my over the last 10 m.y., during which time the active volcanic arc between 33-34°S migrated ~50 km to the east (Figure 3). Stern [3-5] therefore proposed that crustal components were preferentially incorporated in NSVZ compared to CSVZ magmas by increased rates of subduction erosion and mantle source region contamination by subducted components, and not by intra-crustal MASH processes.

Temporal variations in the isotopic compositions of Andean igneous rocks also are not unambiguously related to either changes in crustal thickness or rates of subduction erosion. Below the NSVZ, in the region where the El Teniente deposit formed in the Late Miocene (Figures 2 and 3), the crust has thickened and been uplifted since the Middle Miocene [12-20], and Sr, Nd and Pb isotopic data indicate increased proportions of continental crust in the igneous rocks emplaced through time (Figures 4 and 5; [10,21-24]). However, as described above, the southward migration of the locus of subduction of the Juan Fernández Ridge has also caused, during this same time period, flattening of the angle of subduction, >50 km of eastward migration of the volcanic arc, and increased rates of subduction erosion (Figure 3; [3-5,10,25-27]).

89
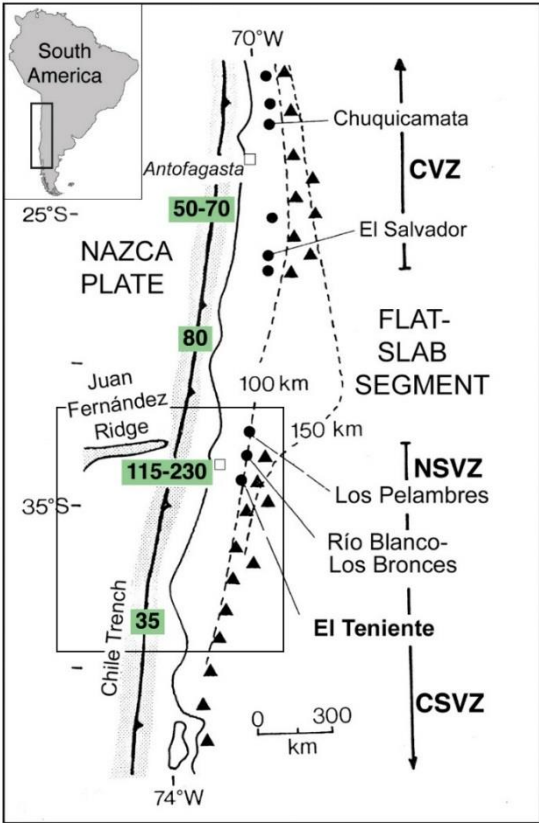
Figure 2. Location map of El Teniente, the two other giant Late Miocene Cu-Mo deposits, Los Pelambres and Río Blanco-Los Bronces, in the Andes of central Chile, and some of the other giant Late Eocene and Early Oligocene Cu-Mo deposits in northern Chile west of the Andean Central Volcanic Zone (CVZ). The area of the figure is indicated by the box in the inset, and the box in the figure shows the region illustrated in Figure 3. The figure also shows tectonic features such as the Chile Trench, which is the boundary between the Nazca and South American plates, and the depth in kilometers (100 and 150 km dashed lines) to the Benioff Zone below South America. The locus of subduction of the Juan Fernández Ridge occurs at the boundary between the Andean Flat-Slab segment, below which the subduction angle is very low as indicated by the depths to the upper boundary of the subducted slab, and the northern and central parts of the Andean Southern Volcanic Zone (NSVZ and CSVZ) of active volcanoes, below which subduction angle is steeper. The numbers in the green boxes are the estimated rates of subduction erosion in $km^3/km/my$ in each region [5]**.** Subduction erosion rates are higher in northern compared to south-central Chile because of the arid conditions in the north, resulting in a trench devoid of sediment, and humid conditions in the south, resulting in a trench filled with sediment [4,5,9]. Rates are highest just south of the locus of subduction of the Juan Fernández Ridge due to the effects of the subduction of this buoyant feature [5,26,27]. (Reprinted from Geology, volume 22, M.A. Skewes and C.R. Stern, Tectonic trigger for the formation of late Miocene Cu-rich breccia pipes in the Andes of central Chile, page 552, Copyright 1994, with fair use permission from the Geologic Society of America.)

109   In summary, the spatial and temporal variations in geologic factors such as crustal thickness and
110   rates of subduction erosion rates do not unambiguously favor MASH versus source region
111   contamination in producing the spatial and temporal isotopic variations that indicate increased
112   incorporation of continental crust in some Andean magmas. An alternative approach to distinguish
113   these two processes is geochemical modelling focused specifically on mafic olivine-bearing basaltic
114   rocks clearly derived from the mantle, without significant evidence for or possibility of intra-crustal
115   contamination. For instance, to produce the northward increase of $^{87}Sr/^{86}Sr$ from 0.7039 to 0.7050 and
116   decrease in ε_{Nd} from >+5 to <-1 observed in the olivine basalts erupted from CSVZ compared to NSVZ
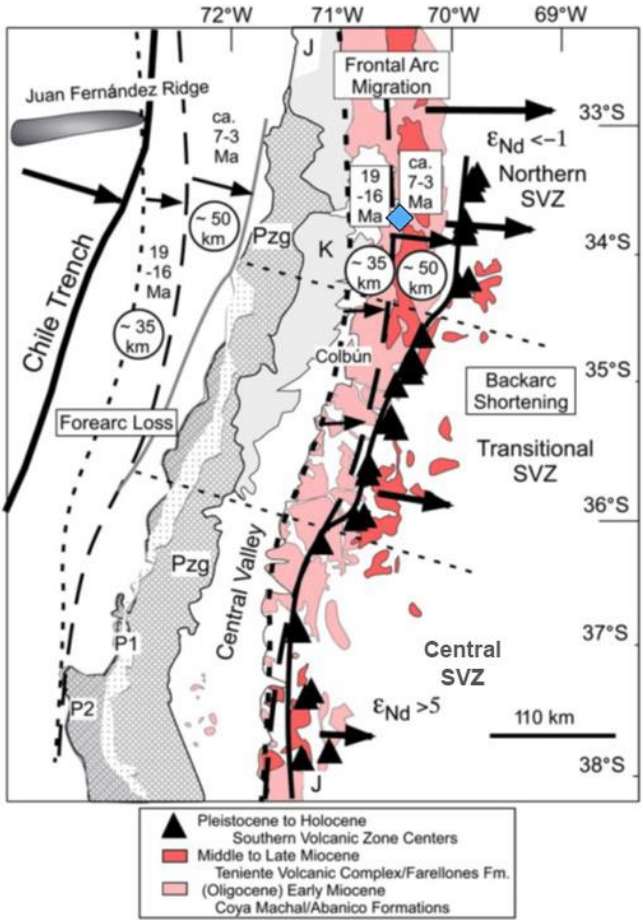
Figure 3. Regional map of central Chile between ~32°S and 38°S, with lines showing correlations of early Miocene to Holocene arc fronts on land and inferred position of corresponding coastlines offshore [10]. Arrows show relative amounts of frontal-arc migration, forearc loss, and backarc shortening. Northwest–southeast trending dashed lines show offsets in the modern volcanic front that separate the Southern Volcanic Zone (SVZ) into the northern, transitional, and central segments [4]. In the active arc region, lines connect outcrop patterns marking early Miocene (pink), middle to late Miocene (red), and the Pleistocene to Holocene volcanic centers of the SVZ (triangles) magmatic fronts. Arrows between the lines indicate inferred distance (given in circles) of frontal-arc migration from 19 to 16 Ma and from 7 to 3 Ma. In the forearc, lines between the trench and the coast show inferred early Miocene (short dashed) and middle to late Miocene (long dashed) coastlines under the assumption that the distance of frontal-arc migration equals the width of missing coast. Arrows between the lines in this region indicate distance (shown in circles) of inferred loss by subduction erosion from ca. 19 to 16 Ma. and 7 to 3 Ma. In the backarc, the length and position of arrows show the location and proportional amounts of crustal shortening over the past 20 my inferred from structural profiles. Also shown are other outcrop patterns that have long been used as evidence for forearc subduction erosion along this margin [6]. The first is the northward narrowing and disappearance of the Paleozoic high pressure (P1) and low pressure (P2) paired metamorphic and granitoid (Pzg) belts along the coast. The second is the presence of Jurassic arc rocks (marked by J) along the coast north of 33°S, but inland near the SVZ at ~38°S. K indicates Cretaceous magmatic rocks. ε_{Nd} is +5 for active SVZ volcanoes south of 36°S, and ≤-1 for those in the northern SVZ north of 34°S, as a result of increased mantle source region contamination by subducted crust due to the northward increase in the rate of subduction erosion associated with the subduction of the Juan Fernández Ridge at 33°S [3-5]. El Teniente occurs at the blue diamond. (Reprinted from Geologic Society of American Bulletin, volume 117, S.M. Kay et al., Episodic arc magmatism, crustal thickening, subduction erosion, and magmatism in the south-central Andes, page 83, Copyright 2005, with fair use permission from the Geologic Society of America.)

144   volcanoes (Figures 3-5), would require intra-crustal assimilation (MASH) of >40 wt % of Andean crust
145   (Figure 4; [3,10,21,22]) because of the relative high Sr = >450 ppm and Nd = 9 ppm of Andean basalts.
146   For NSVZ olivine basalts with ~50 wt % SiO_2, but with no macro or microscopic evidence of crustal
147   xenoliths or xenocrysts, this is considered to be an unacceptable large amount of crustal assimilation,
148   as it would increase SiO_2 to ~60 wt %. In contrast, because of the relatively low Sr = 36 ppm and Nd
149   = 1.8 ppm of Andean subarc mantle, these variations could be produced by incorporation in the
150   mantle source region of only 5 wt % more subducted crust and sediment below the NSVZ (Figure 4),
151   where current subduction erosion rates are estimated as between 115 to 230 km^3/km/my (Figure 2),
152   than the 1 wt % estimated to have been incorporated in the mantle below the CSVZ, where
153   subduction erosion rates are estimated as only ~35 km^3/km/my (Figure 2).

154
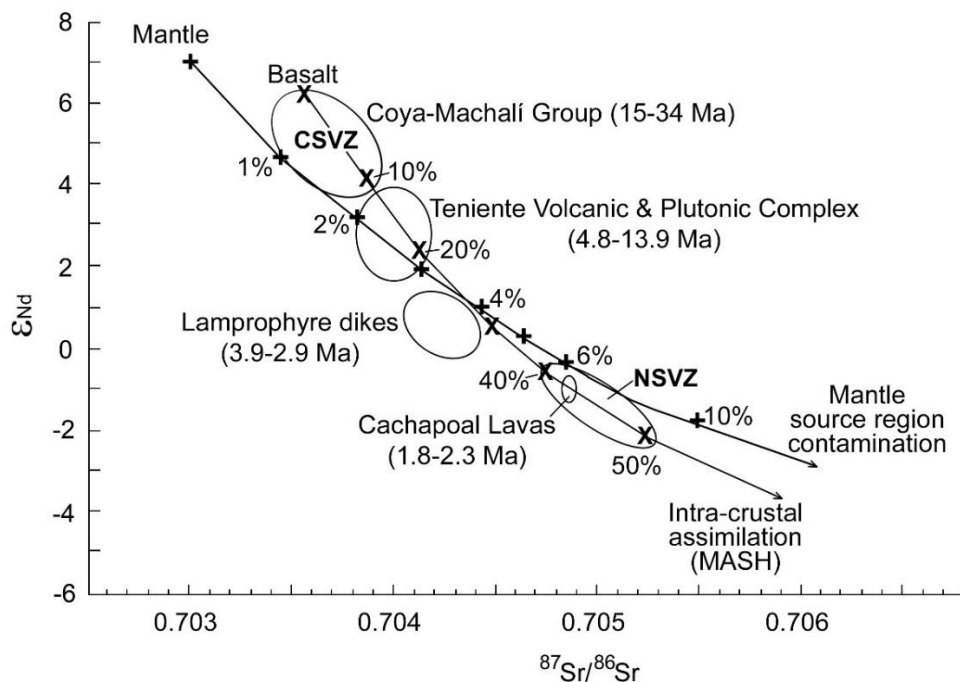
Figure 4. Sr versus Nd isotopic values of the various groups of igneous rocks of different ages in a transect across the Andes at the latitude of El Teniente (34°S; [10,14,17,21-24]). The figure illustrates both a source region contamination model of primitive mantle (+'s, Sr=36 ppm with ^{87}Sr/^{86}Sr=0.703 and Nd=1.8 ppm with ε_{Nd}=+7; [21]) mixed with various proportion of subducted crust and sediment (Sr=380 ppm with ^{87}Sr/^{86}Sr=0.70763 and Nd=42.3 ppm with ε_{Nd}= -5.1), and also a MASH model for a Coya-Machalí basalt (x's, Sr=450 ppm with ^{87}Sr/^{86}Sr= 0.7035 and Nd=9 ppm with ε_{Nd}= +6) assimilating various proportion of Paleozoic-Triassic Andean granite basement (Sr=350 ppm with ^{87}Sr/^{86}Sr=0.7075 and Nd=20 ppm with ε_{Nd}= -6; [10]) Both models reproduce the isotopic compositions of the progressively younger rocks in the transect, but the latter model requires assimilation of unacceptably high proportions of granite crust and is inconsistent with generation of primitive low SiO_2 olivine-bearing mafic rocks in each age group (Figure 5), as well as the progressively higher Sr content of the sequentially younger rocks, which is due instead to decreasing degrees of partial mantle melting [3-5,10] associated with decreasing volume of magmas erupted through time at this latitude in the Andes. (Reprinted from Geologic Society of American Bulletin, volume 117, S.M. Kay et al., Episodic arc magmatism, crustal thickening, subduction erosion, and magmatism in the south-central Andes, page 78, Copyright 2005, with fair use permission from the Geologic Society of America.)

171   Similar temporal isotopic changes as those observed between recently erupted CSVZ
172   and NSVZ basalts occurred between the Miocene and Pliocene in igneous rocks associated
173   with the El Teniente Cu-Mo deposit (Figures 3-5; [21-23]). As a contribution to the
174   understanding of Andean magmagenesis and its relation to the formation of the giant El
175   Teniente ore deposit, we have determined the Hf isotopes of igneous rocks ranging in age

176 from ≥8.9 to 2.3 Ma from the area of the deposit. These samples (Table 1) include an olivine
177 basalts (8.9 Ma), an olivine lamprophyre (3.1 Ma), and an olivine-bearing basaltic andesites
178 (2.3 Ma), as well as other mafic and felsic plutons associated with the deposit. The data
179 obtained provide information about the temporal evolution of their magmatic sources from
180 the Late Miocene to Pliocene, and constrain the relative role of MASH and mantle source
181 region contamination processes in the generation of Andean magmas.

182
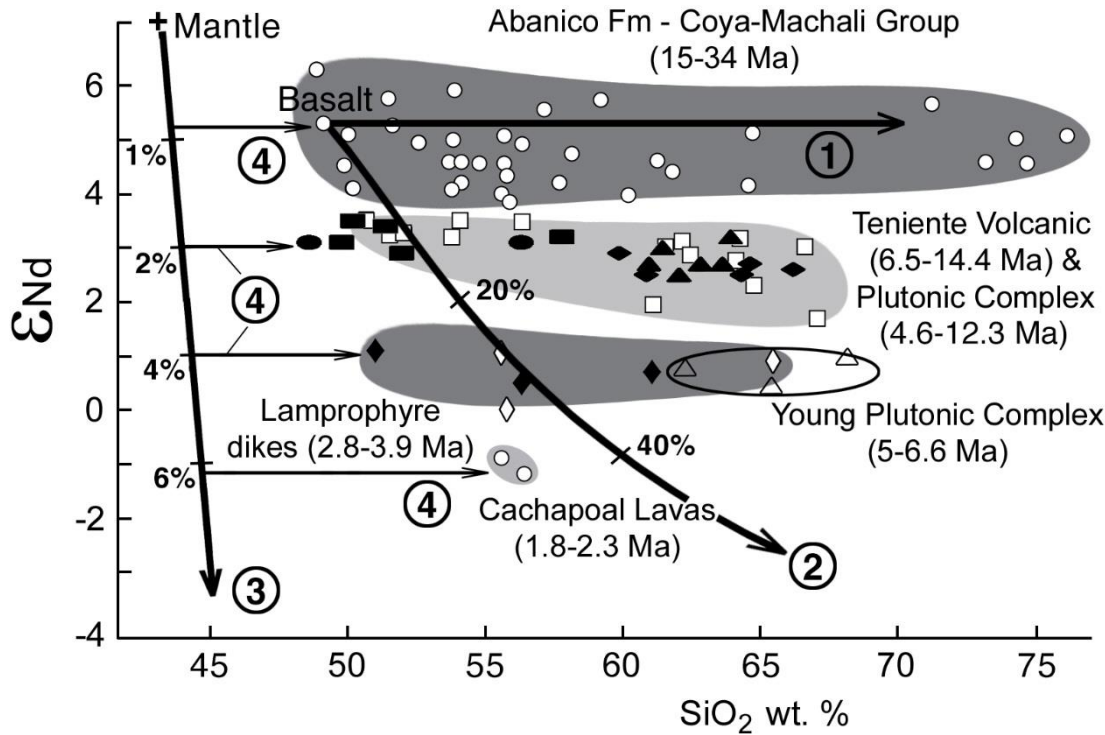
Figure 5. Published values of ε_{Nd} vs SiO_2 (wt %) for igneous rocks of different ages from the transect
across the Andes at the latitude of El Teniente (34°S; open symbols [10,14,17,21-24], compared with
values for samples of the host-rocks in the deposit (filled symbols including the Teniente Mafic
Complex (■), Sewell Tonalite (▲), felsic porphyries(♦), and Porphyry A granitoid (●); [23]). Three
curves illustrate the progressive changes in SiO_2 and ε_{Nd} for 1) crystal-liquid fractionation without
assimilation, 2) intra-crustal assimilation combined with crystal-liquid fractionation (MASH), and 3)
mantle source region contamination. Crystal-liquid fractionation increases SiO_2 without changing
isotopic composition. MASH increases SiO_2 as ε_{Nd} decreases. Source region contamination decreases
ε_{Nd} in the mantle, but mantle partial melting (curves 4) for the modified mantle still produces mafic
olivine-bearing basalts and lamprophyres. Tic marks along each curve indicate the same amount of
crustal contamination as in the MASH and source region contamination models illustrated in Figure
4. Although the youngest felsic plutons in the deposit are the same age (7.1 to 4.6 Ma) as rocks from
the regionally defined Young Plutonic Complex of small barren plutons outside the deposit (6.6 to 5
Ma; [10]), they are isotopically similar to the older host-rocks of the deposit as well as to Teniente
Volcanic and Plutonic Complex rocks. This is due to the fact that they formed above a large magma
chamber within which mantle-derived magmas were mixed, stored and homogenized (but without
crustal assimilation), so that the temporal isotopic changes in these mantle-derived magmas through
time are not observed in the progressively younger felsic plutons within the deposit as a result of the
large volume of the magma chamber into which these mantle-derived magmas mixed. In contrast, the
small barren plutons of the Young Plutonic Complex outside the deposit do reflect these temporal
changes in isotopic composition because they do not form above such a large magma chamber.
(Reprinted from Geologic Society of American Bulletin, volume 117, S.M. Kay et al., Episodic arc
magmatism, crustal thickening, subduction erosion, and magmatism in the south-central Andes, page
80, Copyright 2005, with fair use permission from the Geologic Society of America.)

207   **Table 1.** Samples analyzed. Rock types, SiO_2, $^{87}Sr/^{86}Sr$, $^{143}Nd/^{144}Nd$, and ε_{Nd} from [21-23]. $\varepsilon_{Hf(t)}$ from [37].

Sample #	Rock Type	Age Ma	SiO$_2$ wt %	^{87}Sr/^{86}Sr	^{143}Nd/^{144}Nd	ε_{Nd}	$\varepsilon_{Hf(t)}$
Late Miocene (≥8.9 Ma) mafic host rocks							
EX-2004-04	ol basalt	8.9	51.9	0.70405	0.512782	2.9	
1411-1630	gabbro	≥8.9	51.1	0.70396	0.512818	3.5	
540-2082	basalt	≥8.9	51.3	0.70404	0.512813	3.4	
QT-4	basalt	≥8.9	49.7	0.70421	0.512798	3.1	
Late Miocene to Early Pliocene (7.1 to 4.8 Ma) felsic plutonic rocks							
Ttc5	Sewell tonalite	7.1	63.7	0.70386	0.512770	2.7	7.9
1473-970	Porphyry A	5.7	48.5	0.70409	0.512799	3.1	
1446-266	Porphyry A	5.7	56.3	0.70406	0.512795	3.1	7.7
1300-403	Teniente dacite	5.3	66.3	0.70402	0.512762	2.6	7.2
1394-92	latite dike	4.8	60.9	0.70405	0.512785	2.5	6.9
Pliocene (3.8 to 2.3) lamprophyres and basaltic andesites							
Ttc1	hbl lamprophyre	3.8	56.3	0.70425	0.512660	0.7	
AS-2003-1	ol lamprophyre	3.1	51.3	0.70425	0.512700	1.2	
PVF1	ol basaltic andesite	2.3	55.6	0.70485	0.512580	-1.1	

208   **2. Geologic Background**

209   *2.1. El Teniente Cu-Mo deposit*

210   The giant El Teniente Cu-Mo deposit, located in central Chile (34°05'S, 70°21'W; Figures 2 and
211   3) is one of the largest such deposits in the world [28-38]. It is the southernmost in a belt of three giant
212   Late Miocene Cu-Mo deposits which also includes Los Pelambres and Río Blanco-Los Bronces [39,40].
213   El Teniente has been described as a porphyry deposit formed around the central Teniente Dacite
214   Porphyry dike (Figure 6; [30]), or alternatively as a magmatic-hydrothermal breccia deposit formed
215   either in association with the intrusion of dacite to diorite dikes [36] or by the generation of multiple
216   large mineralized breccias, including the central Braden breccia pipe, by exsolution of high-
217   temperature mineral-rich magmatic-hydrothermal fluids from the roof of an underlying large, long-
218   lived and vertically stratified magma chamber recharged from below by mantle-derived magmas
219   [23,32,33,38]. The two other Miocene deposits in this belt are also characterized by the presence of
220   multiple large mineralized magmatic-hydrothermal breccias [38-42].
221   Pb, S, O and H isotopic studies of the igneous rocks and ore minerals in the deposit indicate that
222   El Teniente is clearly an orthomagmatic deposit, with Cu, Mo and S being derived from the associated
223   igneous rocks [32,33,39,43-45]. Igneous rocks spatially related with the deposit range in age from mid
224   Tertiary to Pliocene. Over this time period the volume of magmatic rocks decreased progressively
225   [22,23,38,39], and in the Pliocene the locus of Andean arc magmatism at the latitude of El Teniente
226   (34°S), near the current northern end of the Andean Southern Volcanic Zone (NSVZ; Figures 2 and
227   3), migrated ~50 km to the east as the subduction angle flattened [25]. This, we suggest, was due to
228   the southward migration of the locus of subduction of the Juan Fernández Ridge [21,25-27,38,39].
229   The igneous rock in the vicinity of El Teniente include continental volcanic rocks, up to 3300 m
230   thick, of the Oligocene to Early Miocene (≥15 Ma) Coya-Machali or Abanico Formation (Figure 3;
231   [15,46,47]), erupted above thin (<30 km) crust, or in a transtensional intra-arc basin [48]. These formed
232   by relatively high degrees of partial melting of subarc mantle modified to a small degree by the influx
233   from below of slab-derived components (Figure 5; [10,17,46]). This is indicated by their low La/Yb
234   ratios (2-6), as well as their low initial $^{87}Sr/^{86}Sr$ (0.7033-0.7039) and high ε_{Nd} (+6.5 to +4; Figures 4 and
235   5). Although the Coya-Machali Formation volcanic rocks do not crop out either within or in the
236   immediate vicinity of the El Teniente deposit (Figures 3 and 6), these rocks occur both to the west and
237   the east of the deposit, and they almost certainly also occur at depth below the deposit.

238
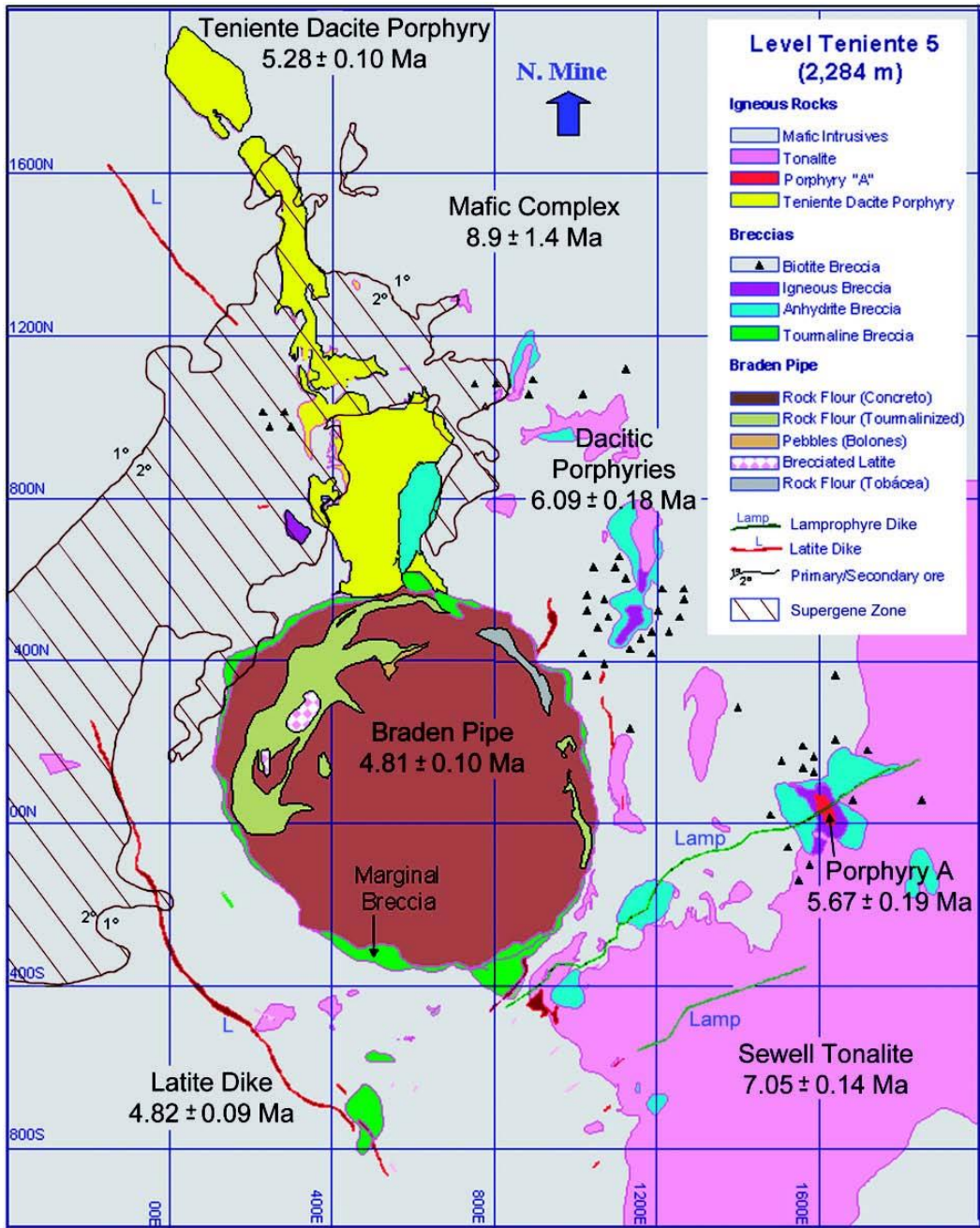
Figure 6. Geological map of level Teniente 5 (2284 m above sea level) in the mine [32,33]. The Dacitic Porphyries north of the Sewell Tonalite, are mapped as a distal portion of this pluton, although they are younger [34] and have an independent origin [36]. The spatial extent of biotite breccias is projected onto this level from where they have been mapped between levels Teniente 4 and 8. (Reprinted from Journal of Petrography, volume 52, C.R. Stern et al., Magmatic evolution of the giant El Teniente Cu-Mo deposit, central Chile, page 1594, Copyright 2011, with permission from Oxford University Press.)

Extrusive rocks of the Miocene Farellones Formation, locally referred to as the Teniente Volcanic Complex [10], are the oldest rocks exposed in the immediate area surrounding the deposit (Figure 3). The Farellones Formation, a sequence of >2500 m of lavas, volcanoclastic rocks, dikes, sills and stocks of basaltic to rhyolitic composition, was erupted after an Early Miocene (19-16 Ma episode of crustal deformation, thickening and uplift [10,14]. The Teniente Volcanic Complex near the deposit has been correlated with the upper part of this formation and dated between 14.4 and 6.5 Ma [10,31]. No extrusive rocks with ages less than 6.5 Ma have been found within the El Teniente deposit.

252   The Teniente Volcanic Complex consists of tholeiitic to calc-alkaline extrusive rocks, which plot
253   in the medium to high-K group of convergent plate boundary arc magmas [10]. Mafic rocks of the
254   Teniente Volcanic Complex generally have higher La/Yb (4-9) compared with rocks of the older Coya-
255   Machali Formation, and mafic, intermediate and silicic rocks also have higher initial $^{87}Sr/^{86}Sr$ (0.7039-
256   0.7041; Figure 4) and lower initial ε_{Nd} (+2.7 to +3.6; Figures 4 and 5). These differences are interpreted
257   to represent a change from magma genesis below relatively thin continental crust during the mid-
258   Tertiary, when the Coya-Machali Formation was generated, to conditions of thickened continental
259   crust when the Teniente Volcanic Complex formed in the Middle to Late Miocene.
260   The extrusive rocks of the Teniente Volcanic Complex were intruded between ~8.9 and 4.6 Ma,
261   during a Late Miocene episode of further crustal deformation, thickening and uplift, [10,14,31,34,48],
262   by gabbro, diabase, diorite, tonalite, latite, and dacite porphyry plutons of the Teniente Plutonic
263   Complex. Within the immediate area of the deposit (Figure 6) these include 1) the >50 km³ Teniente
264   Mafic Complex (8.9 ± 2.4 Ma) of mafic intrusives with the form of a laccolith 2000 m thick in the center
265   of the deposit; 2) the equigranular holocrystalline Sewell Tonalite complex (7.05± 0.14 Ma), with an
266   estimated volume of ~30 km³ [23]; and 3) a series of much smaller volume (<1 km each) dacite and
267   diorite porphyries (6.09±0.18 Ma), the unusual Cu- and S-rich anhydrite-bearing Porphyry A stock
268   (5.67±0.19 Ma; [49]), the Teniente Dacite Porphyry dike (5.28±0.10 Ma), a few latite dikes (4.82±0.09
269   Ma), and finally a small dacite porphyry (4.58±0.10 Ma). These intrusive rocks have isotopic
270   compositions similar to Teniente Volcanic Complex extrusives (Figures 4 and 5).
271   Multiple Cu-mineralized magmatic-hydrothermal breccia pipes were emplaced into these
272   plutonic rocks during the same time period as the felsic porphyry intrusions, between at least 6.3 and
273   4.4 Ma (Figure 6). Post-mineralization phases include high-MgO (≥7.50 wt %) olivine (Fo88) and
274   hornblende lamprophyres (3.8 to 2.9 Ma; 10,22,31,34]) and olivine (Fo64) basaltic andesite (MgO≥4.5
275   wt %) lavas in the valley of the Cachapoal river just west of the El Teniente deposit (2.3 Ma; 21]). After
276   this the locus of Andean arc magmatism migrated eastwards ~50 km (Figure 3).

2.1. Previous Hf isotopic studies

278   Hf isotopes have previously been determined in zircons from felsic plutons both within [37] and
279   in the vicinity [50] of the El Teniente deposit (Figure 7). The Hf isotopic composition of zircons in six
280   samples of felsic plutons within the deposit, that range in age from 7.1 to 4.8 Ma, have overall high
281   initial average of $\varepsilon_{Hf(t)}$ = +7.4 ± 1.2 and range from +6 to +10 (Table 1), which rules out significant
282   crustal contamination [37]. There was little change in these compositions during this time, but the
283   older four plutons (7.1 to 6.1 Ma) average $\varepsilon_{Hf(t)}$ = +7.8, while the younger Teniente Dacite Porphyry
284   (5.3 Ma) has $\varepsilon_{Hf(t)}$ = +7.2 and the youngest latite dike (4.8 Ma) has $\varepsilon_{Hf(t)}$ = +6.9 (Table 1), so some small
285   but significant temporal change, with decreasing $\varepsilon_{Hf(t)}$ through time, is apparent.
286   Hf isotopic compositions were also determined in four barren Middle and Late Miocene plutonic
287   complexes in the vicinity of El Teniente [50]. These can be divided into an older group (~15 Ma) and
288   a younger group (10 to 12 Ma), both groups being older than the felsic plutons within the El Teniente
289   deposit (Figure 7). The older group is characterized by quartz monzogabbroic compositions with 54.0
290   to 57.5 wt % SiO₂, while the younger group are quartz monzodioritic with higher SiO₂ from 61.6 to
291   66.8 wt %. $\varepsilon_{Hf(t)}$ for the older group ranges from +9.8 to +13.7 and averages +11.6 (Figure 7), while $\varepsilon_{Hf(t)}$
292   for the younger group has a lower range of +7.6 to +8.5 and a lower average of +8.0. These differences
293   are also associated with increasing ε_{Os} from +32 to +160 for the older compared to the younger group.
294   Both the Hf and Os isotopic data suggests increasing incorporation of crustal components with time,
295   and the younger plutons, which have higher SiO₂, are noteworthy for the presence of abundant mafic
296   enclaves indicating intra-crustal (MASH) assimilation on a macroscopic scale. These are absent from
297   the older plutonic group which have more primitive isotopic compositions and lower SiO₂.
298

299
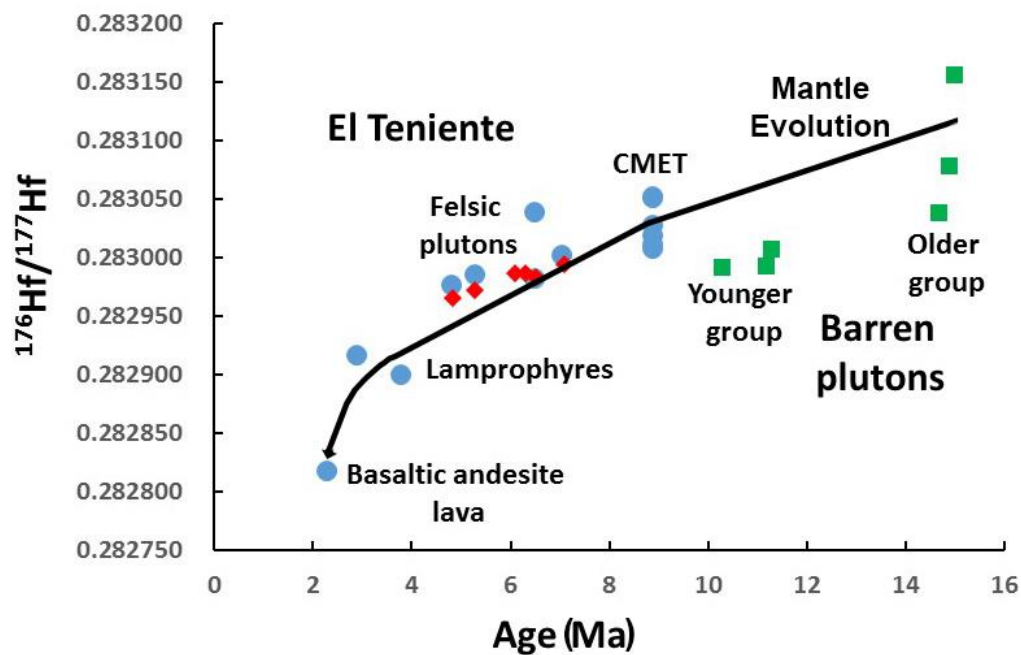
Figure 7. [176]Hf/[177]Hf versus age (Ma) for samples from El Teniente (blue circles from Table 4; red diamonds from [37]) and Middle Miocene barren plutons in the same general area (green squares from [50]). The size of the symbols is greater than the error in the [176]Hf/[177]Hf values. The mantle isotopic evolution line is drawn from the average of the older group of Middle Miocene barren plutons through the Late Miocene Teniente Mafic Complex (CMET) olivine basalts and gabbros, and then to the Pliocene olivine lamprophyres and olivine-bearing basaltic andesites, ignoring the younger group of barren plutons because these have macroscopic evidence for intra-crustal assimilation [50]. The amount of subducted crust plus sediment added to the mantle to generate this line is indicated in Figure 9.

Hf and Nd isotopic compositions have also been determined for five Late Miocene to Pliocene (8.3 to ~3 Ma) plutons from the Eastern Principal Cordillera ~40 km east of El Teniente (Figure 8; [24]). These have lower more radiogenic $\varepsilon_{Hf(t)}$ (+4 to -4) and ε_{Nd} (+3 to 0) than the felsic plutons in El Teniente. Crustal-contamination (MASH) processes involving assimilation of Paleozoic and Mesozoic basement rocks are evidently involved in the genesis of the igneous rocks from the Eastern Cordillera (Figure 8), both because some contain zircon crystal with older (Paleozoic) inherited cores and others have wide ranges (+1 to -4) of zircon $\varepsilon_{Hf(t)}$ values [24]. However, it has also been suggested that the low ε_{Nd} values of the Pliocene olivine lamprophyres (+1.2 to +0.7) and olivine-bearing basaltic andesites (-1.1; Figures 4 and 5; Table 1; [21-23]) emplaced in the Western Cordillera in the vicinity of El Teniente reflect a westward propagation of the Eastern Cordillera magmatic isotopic signatures, caused by westward thrusting and material transport of the Eastern Cordillera basement under the Western Cordillera in the Pliocene (Figure 8; [24]). We disagree with this interpretation as it fails to take into account the fact that the Pliocene high-Mg olivine lamprophyres, as well as the olivine-bearing basaltic andesite lavas, are likely to be mantle-derived, without significant crustal contamination. For high-Mg olivine lamprophyres in general, an origin by hydrous (6-16 wt % H_2O) melting of mantle has been suggested [51-55]. As discussed in more detail below, we therefore interpret the temporal change in both $\varepsilon_{Hf(t)}$ and ε_{Nd} to lower more radiogenic values for Pliocene olivine-bearing mafic rocks associated with El Teniente in the Western Cordillera as reflecting a progressive change in mantle composition due to subduction of increased proportions of continental crust, and not to intra-crustal (MASH) contamination processes.
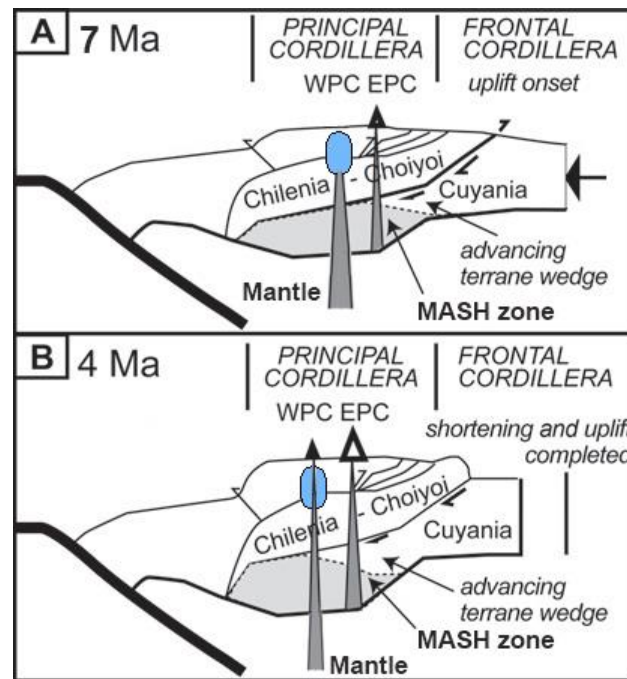
Figure 8. Schematic profiles [18-20,24] of crustal evolution of the Andes of central Chile and Argentina at 7 Ma (A) and 4 Ma (B). Evolution is characterized by increased shortening rates along the eastern flank of the orogenic belt after 7 Ma, where the Chilenia-Choiyoi block overrides the Cuyania terrane, producing uplift of the Frontal Cordillera. This also produced increasing crustal thickness which led to uplift of the entire belt. Deformation amounts suggest that the Cuyania block descended immediately below the eastern part of the magmatic arc, changing composition of the base of the crust and thus changing the crustal magmatic source (MASH zone) below the Eastern Principle Cordillera (EPC). However, below the Western Principle Cordillera (WPC), mafic magmas continued to rise from the mantle without intra-crustal assimilation in a MASH zone. Between 7 to 4 Ma, these mantle-derived mafic magmas did not reach the surface, but were mixed, stored and homogenized in a large magma chamber (blue) below El Teniente. Within this chamber the felsic plutons of the deposit developed without crustal assimilation and above it the mineralized breccias in the deposit were emplaced (see Figure 10). As subduction angle flattened and magma supply from the mantle decreased this chamber solidified. After 4 Ma, high-MgO olivine lamprophyres and olivine-bearing basaltic andesites, derived from a mantle hydrated and isotopically modified by increased proportions of subducted crust and sediment (Figure 7), rose through the now crystallized magma chamber, without any intra-crustal assimilation, to form dikes and lavas. (Reprinted from Geology, volume 41, M. Muñoz et al., Isotopic shifts in the Cenozoic Andean arc of central Chile: records of an evolving basement throughout cordilleran arc mountain building, page 933, Copyright 2013, with fair use permission from the Geologic Society of America.)

Finally, $\varepsilon_{Hf(t)}$ values ranging from +6.9 to + 9.6 were determined for 8 plutonic rocks between the ages of 28.1 and 11.5 Ma from the region north of El Teniente between 32-33°S [47]. The oldest sample, a dacite sill (sample Ab-143; 28.1 Ma), which has $(^{87}Sr/^{86}Sr)i = 0.70661$ and is likely to have assimilated crustal material, has lower $\varepsilon_{Hf(t)}$ of +7.8 than younger (22.2-17.7 Ma) gabbro, microgabbro and granodiorite samples which average $\varepsilon_{Hf(t)}$ of +8.9. All the still younger plutons have lower ε_{Hf} and the youngest (11.5 Ma; sample Z-132) has an $\varepsilon_{Hf(t)}$ of +7.0. This suggest decreasing $\varepsilon_{Hf(t)}$ with time beginning after ~17 Ma, and possibly before this time. Since these samples are all north of the current locus of subduction of the Juan Fernández Ridge, in an area where ridge subduction, decreasing subduction angle, eastward arc migration and increased rates of subduction erosion all happened earlier than at the latitude of El Teniente, we do not consider them appropriate for evaluating the temporal evolution of the mantle source of El Teniente magmatic rocks.

361   **2. Samples and Methods**

362   Twelve samples were selected for Hf-isotopic analysis (Tables 1-3). These range in age from ≥8.9
363   to 2.3 Ma and include 1) four samples from the Teniente Mafic Complex, including one olivine (Fo74)
364   basalt, one gabbro and two other olivine-free basalts (Table 2); 2) five syn-mineralization felsic
365   intrusions that range in age from 7.1 to 4.8 Ma (Table 3), including four samples previously analyzed
366   for Hf isotopes in zircon [37]; and 3) three post-mineralization samples that range in age from 3.8 to
367   2.3 Ma, including one high-MgO (7.9 wt %; Ni ~190 and Cr ~390 ppm) olivine (Fo88) lamprophyre
368   [22] and one olivine-bearing (Fo64) basaltic andesite (Table 2). All the sample have been previously
369   analyzed for major and trace element contents and Sr and Nd isotopic compositions [21-23].

370   Ground sample weighing ~200 mg was decomposed in 15 ml screw-top Savillex Teflon® vials
371   with a 1:1 mixture of 27 N HF and 16 N HNO_3 at ~150°C for 5 days. The closed beakers were repeated
372   placed in an ultrasonic bath during the course of digestion to enhance digestion efficiency. Each
373   individual sample was carefully checked to make sure no visible solid residue was left in the Teflon
374   beakers, and a clear solution was obtained for each run. The sample solutions were evaporated to
375   incipient dryness and redissolved first by 2 ml 4 N HCl and then by 1 N HCl. The dried samples were
376   then taken into solution by 1 ml 2N HCl and 8 ml 6 N HCl–0.2 N HF prior to chemical separation.
377   Hafnium was separated from the matrix elements by two columns packed with Ln-spec resin (50−100
378   μm) from Eichrom Industries. Major elements and REE were eluted by 3 N HCl and 6 N HCl, and
379   then Ti and Zr were eluted using a 2 N HCl–0.1 N HF mixture. Hafnium was collected from the
380   column with 2 N HCl and 0.2 N HF, and was then evaporated to incipient dryness and taken up by
381   2 N HCl–0.2 N HF. The chromatographic procedures are repeated again on the same column for
382   further purification. Hafnium isotopes were measured on a Nu Plasma II multi-collector ICP-MS
383   connected to an Aridus II desolvator and an enhanced sensitivity system with Ni 325-294 skimmer
384   cone and Ni 319-646 sampler cone. The measured $^{176}Hf/^{177}Hf$ values were normalized for mass
385   fractionation based on $^{179}Hf/^{177}Hf = 0.7325$. Long-term mean value for the Hf standard JMC475 in the
386   laboratory is $^{176}Hf/^{177}Hf = 0.282164 \pm 8$ (n = 55). The $^{176}Lu/^{177}Hf$ ratio was calculated from the Lu and
387   Hf contents determined by ICP-MS techniques by Activations Laboratories (Canada).

388   **4. Results**

389   The $\varepsilon_{Hf(t)}$ determined on the bulk-rock samples of the 7.1 to 4.8 Ma felsic plutons (Table 4) are
390   similar within analytical error to those determined previously on zircons for the same plutons [37].
391   The good match of isotopic compositions indicates that Hf isotopes were not fractionated by any
392   potential undigested phases. The $\varepsilon_{Hf(t)}$ for all our twelve samples ranges from an average of +9.1 for
393   the four samples of ≥8.9 Ma Teniente Mafic Complex basalts and gabbros down to +1.6 for the 2.3 Ma
394   olivine-bearing basaltic andesite lava flow (Table 4), which is the last manifestation of magmatic
395   activity in the region of El Teniente prior to the eastward migration of the volcanic arc. This implies
396   a drop of 7.5 $\varepsilon_{Hf(t)}$ units over this 6.6 m.y. interval. Although Muñoz et al. [37] concluded that there
397   was no change in $\varepsilon_{Hf(t)}$ among the felsic plutons emplaced between 7.1 to 4.8 Ma, the new data for
398   samples formed over the larger ~6.6 m.y. interval from ≥8.9 to 2.3 Ma indicates that there was a clear
399   progressive decrease in $\varepsilon_{Hf(t)}$ with decreasing age (Figure 7).

400   Muñoz et al. [37] suggested that the full $\varepsilon_{Hf(t)}$ range of +6 to +10 of the 7.1 to 4.8 Ma felsic plutons
401   is "identical to preceding Cenozoic barren magmatic activity in Central Chile." However, although
402   their average $\varepsilon_{Hf(t)}$ value of +7.4 (Table 1) is only somewhat lower than the younger group (10-12 Ma)
403   of barren plutons, for which macroscopic and Os isotopic evidence of upper crustal assimilation has
404   been documented, it is significantly lower than the older group (~15 Ma; Figure 7). When the $\varepsilon_{Hf(t)}$ of
405   the older ~15 Ma group of barren plutons in the region, which average +11.6 [50], is taken into account,
406   it is clear that $\varepsilon_{Hf(t)}$ values have not remained constant through time (Figure 7). In fact, there has been
407   an overall decrease of 10 $\varepsilon_{Hf(t)}$ units for igneous rocks emplaced in the vicinity of El Teniente in the
408   12.7 m.y. period from the Middle Miocene to the Pliocene.

409

Table 2. Major and trace-element (in ppm) compositions of mafic rocks from El Teniente [21-23].

Sample	Pre-mineralization samples ≥8.9 Ma.				Post-mineralization samples ≤3.9 Ma.		
	EX2004-04	1411-1630'	540-2082'	QT-4	AS2003-01	TTc-1	PVF1
SiO_2	51.94	51.08	51.3	49.65	51.31	56.30	56.50
TiO_2	0.92	1.09	1.07	1.00	1.01	0.85	1.10
Al_2O_3	18.19	17.07	18.68	17.96	15.97	16.90	16.90
Fe_2O_3		11.04	9.89		7.82	3.60	2.70
FeO	8.78			9.90		2.00	5.10
MnO	0.13	0.08	0.15	0.53	0.13	0.06	0.12
MgO	5.71	5.75	5.23	5.29	7.92	3.30	4.80
CaO	7.87	6.58	9.00	6.56	7.77	5.80	7.20
Na_2O	3.82	2.15	3.21	4.30	3.39	4.61	3.63
K_2O	1.01	2.56	1.00	1.03	1.06	1.60	2.10
P_2O_5	0.20	0.19	0.22	0.22	0.26	0.29	0.33
LOI	0.98	1.46	1.07	4.53	2.04	5.10	0.68
Total	99.55	99.05	100.82	100.97	98.66	100.41	101.16
Cs	7	18	5.3	0.8	8.5	7.7	2.7
Rb	26	159	54	29	21	40	60
Sr	468	383	535	595	680	916	566
Ba	235	100	158	310	345	460	471
La	13.4	11.4	9.20	11.5	13.6	17.5	22.3
Ce	30.3	26.4	20.3	26.5	31.0	40.6	50.0
Pr	3.72	3.40	2.80	3.20	3.98	5.12	
Nd	16.6	15.5	13.3	15.8	17.7	22.0	31.9
Sm	4.00	3.71	3.30	3.90	3.90	4.09	6.52
Eu	1.22	1.04	1.29	1.16	1.20	1.09	1.36
Gd	3.70	3.11	3.50	3.40	3.30	3.07	
Tb	0.60	0.51	0.60	0.60	0.50	0.38	0.66
Dy	3.40	3.00	3.30	3.30	2.82	1.71	
Ho	0.70	0.60	0.60	0.70	0.50	0.31	
Er	1.90	1.60	1.90	2.00	1.50	0.84	
Tm	0.28	0.24	0.30	0.27	0.21	0.13	
Yb	1.70	1.48	1.70	1.60	1.29	0.80	2.32
Lu	0.25	0.21	0.24	0.25	0.18	0.12	0.30
Y	15	15	17	17	14	13	24
Zr	86	56	73	74	110	129	196
Hf	2.7	1.7	1.9	2.5	3.1	3.5	5.0
Th	3.7	1.2	1.3	2.9	2.6	2.4	6.9
Sc	21	30	27	24	23	11	18
Cr	268	292	263	41	387	77	
Ni	134	198	75	30	188	78	
Cu	115	1325	204	20	94	85	

410

Table 3. Major and trace-element (in ppm) compositions of felsic porphyries [23].

Sample	Ttc5	1473-970′	1446-266	1300-403'	1394-92'
SiO$_2$	63.7	48.45	56.34	66.26	60.93
TiO$_2$	0.39	1.01	0.42	0.38	0.63
Al$_2$O$_3$	17.1	18.62	13.86	16.85	17.24
Fe$_2$O$_3$	1.90	7.54	2.74	1.83	2.14
FeO	2.40				
MnO	0.08	0.03	0.02	0.02	0.02
MgO	1.50	4.73	1.41	1.01	1.86
CaO	3.90	5.73	6.72	2.82	4.61
Na$_2$O	4.93	4.33	3.8	5.53	4.76
K$_2$O	2.20	3.63	5.68	2.64	2.23
P$_2$O$_5$	0.21	0.22	0.17	0.14	0.21
LOI	1.80	4.66	7.99	1.95	5.74
Total	100.17	100.39	102.49	99.43	100.37
Cs	6.1	16.3	5.3	1.5	2.7
Rb	96	209	187	66.7	80.5
Sr	699	499	456	699	742
Ba	528	244	601	644	311
La	14.4	10.6	24.1	10.4	14.6
Ce	34.7	21.4	53.7	20.1	30.9
Pr	3.97	2.84	6.29	2.42	4.00
Nd	19.2	13.43	26.12	9.00	15.3
Sm	3.39	3.44	4.63	1.58	2.80
Eu	0.88	1.00	0.79	0.65	0.83
Gd	2.9	2.96	3.17	1.40	2.30
Tb	0.29	0.51	0.38	0.20	0.20
Dy	1.80	2.69	1.89	0.80	1.00
Ho	0.30	0.50	0.34	0.18	0.20
Er	0.90	1.39	0.94	0.50	0.50
Tm	0.12	0.19	0.13	0.07	0.07
Yb	0.92	1.12	0.79	0.40	0.40
Lu	0.11	0.16	0.11	0.06	0.07
Y	11	13	9	5	6
Zr	94	95	81	94	108
Hf	3.2	2.8	3.9	2.4	2.9
Th	4.3	0.8	5.9	2.8	2.3
Sc	6.0	21	2.6	4.0	8.0
Cr	24	<20	<20	11	42
Ni	< 20	<20	<20	34	86
Cu	480	899	2,380	6000	1250

411

412   **Table 4.** Lu-Hf isotopes of the El Teniente samples.

Sample	Lu (ppm)	Hf (ppm)	$^{176}Lu/^{177}Hf$	$^{176}Hf/^{177}Hf$	$2\sigma \times 10^{-6}$	$(^{176}Hf/^{177}Hf)i$	$\varepsilon_{Hf(t)}$
Late Miocene (≥8.9 Ma) pre-mineralization mafic host rocks							
EX-2004-04	0.25	2.7	0.0131	0.283011	3.3	0.283009	8.6
1411-1630	0.21	1.7	0.0175	0.283051	6.1	0.283048	9.9
1411-1630 dup	0.21	1.7	0.0175	0.283051	3.6	0.283048	10.0
540-2082	0.24	1.9	0.0179	0.283007	3.9	0.283004	8.4
540-2082 dup	0.24	1.9	0.0179	0.283027	4.2	0.283024	9.1
QT-4	0.25	2.5	0.0142	0.283018	3.4	0.283016	8.8
Late Miocene to Early Pliocene (7.1 to 4.8 Ma) syn-mineralization felsic plutonic rocks							
Ttc-5	0.11	3.2	0.0049	0.283001	11	0.283001	8.2
1473-970	0.16	2.8	0.0081	0.283039	6.0	0.283038	9.5
1446-266	0.11	3.9	0.0040	0.282981	7.5	0.282981	7.5
1300-403	0.06	2.4	0.0036	0.282984	3.7	0.282984	7.6
1394-92	0.07	2.9	0.0034	0.282976	2.8	0.282976	7.3
Pliocene (3.8 to 2.3) post-mineralization olivine lamprophyres and basaltic andesites							
Ttc1	0.12	3.5	0.0049	0.282900	3.8	0.282899	4.6
AS-2003-1	0.18	3.1	0.0082	0.282916	3.1	0.282915	5.1
PVF1	0.30	5.0	0.0085	0.282817	2.3	0.282816	1.6

413   **5. Discussion**

414   *5.1. Andean magmagenesis*

415   The observed 10 $\varepsilon_{Hf(t)}$ unit decrease for igneous rocks emplaced in the vicinity of El Teniente in
416   the 12.7 m.y. period from the Middle Miocene to the Pliocene is consistent with decreasing $\varepsilon_{Nd(t)}$ from
417   +5 to -1.1, increasing $^{87}Sr/^{86}Sr(i)$ from 0.70376 to 0.70485, and increasing $^{206}Pb/^{204}Pb$ from 18.55 to 18.68
418   determined for these same samples (Figures 4 and 5; [21-23]). These variations imply increasing
419   incorporation of continental crust through time in the magmas that formed these rocks.
420   The fact that the samples include mantle-derived olivine basalts and high-Mg olivine
421   lamprophyres suggests that these continental components were incorporated into their mantle source,
422   and not by intra-crustal contamination (MASH). This suggestion is supported by two other lines of
423   evidence. One is that for all the rocks of variable SiO_2 content within the igneous associations of
424   specific ages identified in the area of El Teniente, the isotopic compositions do not vary as SiO_2
425   increases (Figure 5). The isotopic compositions of the different associations vary through time, but
426   not as a function of SiO_2. This implies that crystal fractionation processes are not combined with intra-
427   crustal assimilation in the generation of the range of rocks from basalts through rhyolites formed
428   during each of these successive magmatic events. Second, models of intra-crustal assimilation
429   (MASH) for Sr and Nd isotopes (Figure 4; [21-23]) indicate that relatively large proportions (>40 wt %)
430   of crust must be assimilated to produce the Sr and Nd isotopic changes observed between mid
431   Tertiary basalts and Pliocene olivine lamprophyres and olivine-bearing basaltic andesites. This is
432   considered to be an unacceptable large amount of crust to be assimilated in olivine-bearing mafic
433   magmas.
434   In contrast, models of mantle source region contamination by subducted crustal components
435   indicates that the Sr and Nd isotopic evolution of the subarc mantle source of the mafic magmas
436   erupted in the vicinity of El Teniente between the mid Tertiary and Pliocene can be produced by the
437   incorporation of increased, but still relatively small proportions of subducted crust and sediment
438   (Figures 4 and 5; [3,10,21-23]). Mid Tertiary Coya-Machali group mafic volcanic rocks require the
439   addition to a primitive subarc mantle of only 1 wt % subducted crust and sediment, while Pliocene
440   olivine lamprophyres and basaltic andesites require the addition of between 4-6 wt % subducted crust
441   to produce an appropriately isotopically modified mantle source.
442   The difference between these intra-crustal assimilation and mantle source region contamination
443   models reflects the relatively high Sr (450 ppm) and Nd (9 ppm) contents of a basalt relative to the
444   crust being assimilated, thus requiring a relatively large proportion of crust to produce the

445   appropriate isotopic leverage. In contrast the low Sr (36 ppm) and Nd (1.8 ppm) contents of the
446   mantle allows a much smaller proportion of subducted crust and sediment to produce the same
447   isotopic leverage (Figures 4 and 5; [3-5,10,21-23]). For the Hf isotopic system, the same logic applies.
448   The olivine basalts and gabbros of the Teniente Mafic Complex contain an average of 2 ppm Hf (Table
449   4), while average upper continental crust contains 5.3 ppm and bulk continental crust 3.7 ppm Hf
450   [56]. In contrast, primitive mantle contains only 0.28 ppm Hf [57], so the proportion of crust needed
451   to modify the Hf isotopic composition of the mantle is small compared to that needed to be
452   assimilated by a basalt.
453   Since the mantle source region contamination model better explains the Sr and Nd isotopic
454   evolution through time of the same olivine-bearing mafic rocks that we have analyzed for Hf isotopes,
455   we also interpret the temporal change in their Hf isotopic compositions to reflect the isotopic
456   evolution of their mantle source affected by increased incorporation of subducted crust and sediment.
457   To quantitatively evaluate the amount of source region contamination to produce these Hf isotopic
458   variations is complicated for two reasons. The first is the inherent complexities involved in
459   subduction zone magmatism, such as the amounts of pelagic, terrigenous and tectonically eroded
460   continental crust being subducted, and the uncertainty in the processes of transfer of these
461   components into the overlying mantle wedge by either dehydration and volatile transport, melting
462   or diapiric uprise of these low density materials. The second is that information is not available for
463   the Hf contents and isotopic compositions of all these different components relevant to
464   magmagenesis in the vicinity of El Teniente, in particular for the coastal and off shore Paleozoic and
465   early Mesozoic crustal rocks being tectonically eroded and subducted.
466   In the central Mexican magmatic belt, west of where subduction erosion rates are estimated as
467   79-88 km^3/km/my, and where Hf concentration and isotopic data are available for both pelagic and
468   terrigenous sediment, as well as coastal continental rocks, Straub et al. [58] concluded that tectonically
469   eroded continental crust, consisting of coastal and off-shore granodiorite plutons, was the dominant
470   control on the isotopic composition of the calc-alkaline arc magmas, and that neither intra-crustal
471   assimilation nor subducted trench sediment played a significant role in the genesis of these magmas.
472   For the El Teniente rocks, we calculated a model assuming for Hf contents the average estimated
473   values for primitive mantle and the average upper crust for the subducted crust and sediment, as
474   well as a low crustal $^{176}Hf/^{177}Hf$ isotopic ratio similar to that determined by Straub et al. [58] for
475   Mexican basement biotite gneisses (Table 5). This model can generate results (Figure 9) consistent
476   with those previously determined for the Sr and Nd isotopic systems for which more published
477   values for the materials involved in Andean magmagenesis are available [10,21-23]. These models all
478   indicate that the addition of 1 wt % subducted crust and sediment can produce an isotopically
479   modified mantle appropriate for the generation of the mid Tertiary Coya-Machali basalts. Addition
480   of progressively greater amounts of 2, 4 and 6 wt % subducted crust and sediment is required to
481   further modify the mantle to produce the Late Miocene Teniente Mafic Complex olivine basalts and
482   gabbros, the Pliocene olivine lamprophyres and younger Pliocene basaltic andesites, respectively.

483   **Table 5.** Parameters used for the mantle modified by subducted crust + sediment model [22].

	Mantle	Crust + Sediment
Sr ppm	36	380
$^{87}Sr/^{86}Sr$	0.7030	0.70763
Nd ppm	1.8	42.3
$^{143}Nd/^{144}Nd$	0.51300	0.51235
Hf ppm	0.28	5.3
$^{176}Hf/^{177}Hf$	0.28320	0.28256

484
485   What can be said unequivocally in support of this model of the isotopic evolution of the subarc
486   mantle underlying El Teniente is that the rate of subduction erosion and amount of Paleozoic and
487   early Mesozoic crust being subducted did increase between the mid Tertiary and Pliocene as the locus
488   of subduction of the Juan Fernández Ridge migrated southward. Prior to impingement of the ridge
489   on the northern end of the SVZ, subduction erosion rates may have been similar to those estimated

490 presently for the central SVZ of 35 km^3/km/my (Figure 2; [5]). Over the last ~10 m.y., as the ridge
491 approached it current position at the northern end of the SVZ (Figures 2 and 3; [26,27]), rates of
492 subduction erosion west of El Teniente increased to possibly as high as between 115 to 230
493 km^3/km/my [5]. This increased rate of subduction erosion must be considered as the most probable
494 cause for the increasingly crustal Hf, Sr, Nd and Pb isotopic signatures in the igneous rocks associated
495 with the El Teniente deposit through time.
496   A second important factor that changed over the same time period, was that the angle of
497 subduction decreased, thus contributing, along with subduction erosion, to the ~50 km eastward
498 migration of the Andean arc in the Pliocene (Figure 3; [10,25]). Decreasing subduction angle reduced
499 the volume of the subarc mantle wedge and resulted in a progressive decrease in the volume of
500 magmas being produced prior to arc migration. Even if the amount of crustal components transferred
501 from the subducted slab into the mantle wedge remained the same through time, which it didn't
502 since subduction erosion rates increased, the decreasing volume of the wedge would result in these
503 components becoming progressively more significant within the wedge. Stern [3-5] and Kay et al. [10]
504 have shown that the decreasing volume of magma erupted in the vicinity of El Teniente through time
505 from the mid Tertiary to Pliocene is consistent with decreasing percent of mantle partial melting as
506 the angle of subduction decreased. This resulted in increasing Sr contents, from 450 to 700-900 ppm
507 in association with increasing ^{87}Sr/^{86}Sr ratios in the sequence of mid Tertiary basalts to Pliocene olivine
508 bearing mantle-derived lamprophyres [22]. Decreased degrees of mantle partial melting may also
509 explain the somewhat higher Hf contents of the small volume of Pliocene olivine lamprophyres (>3
510 ppm) and basaltic andesite lavas (5 ppm) compared to the older Teniente Mafic Complex olivine
511 basalts and gabbros (2 ppm; Table 4). Lamprophyres in general have been attributed to small degrees,
512 relative to basalts, of partial melting of hydrated (6 to 16 wt % H$_2$O) mantle [51-55], H$_2$O being one of
513 the subducted components likely to increase in significance in the mantle wedge as mantle volume
514 decreases.

515   .
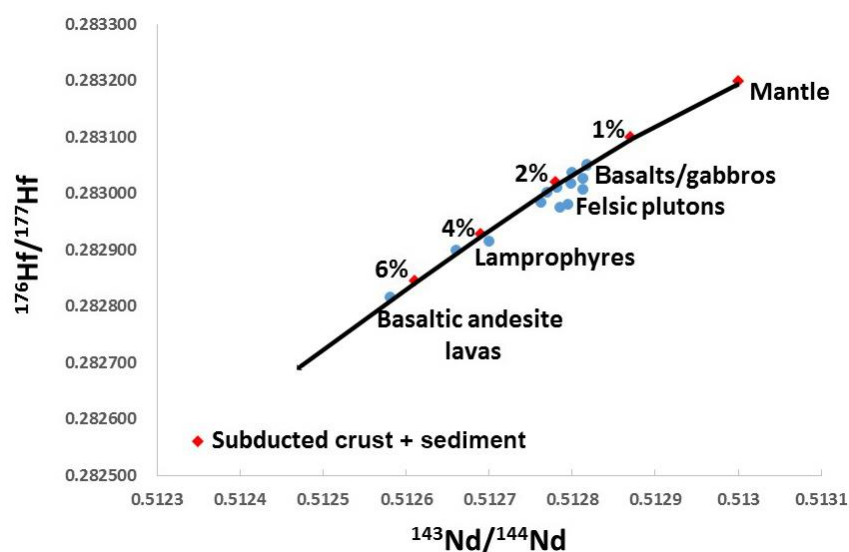
516   **Figure 9.** ^{176}Hf/^{177}Hf versus ^{143}Nd/^{144}Nd for samples from El Teniente (Table 4; blue circles) compared
517   to isotopic values of a primitive mantle (Table 5) modified by the addition of various proportions (red
518   diamonds) of subducted crust and sediment.

519   In summary, the Hf isotopic data are consistent with Sr, Nd and Pb isotopic data, and suggest
520 the incorporation of small but progressively increasing proportions of continental crust in the mantle
521 source of the mafic magmas erupted in the vicinity of El Teniente between 15 and 2.3 Ma. Trench
522 sediment recycling has been confirmed by the detection of cosmogenic ^{10}Be in many, including
523 Andean arc, lavas [59-61], and comprehensive trace-element and isotopic studies have also provided
524 evidence for the incorporation of fore-arc eroded crust in the subarc mantle source of both Andean
525 [3-5,7,8,10,11] and arc volcanoes along other convergent plate boundaries [58,62-64]. The model
526 developed for the El Teniente area suggests that increasing rates of subduction erosion through time

527   has resulted in variable, but nevertheless relatively small (1 to ≤6 %) amounts of subducted crust
528   having significantly affecting the isotopic composition of the mantle source of the mafic magmas
529   through time. Models for magmagenesis in other arcs, for instance the central Mexican volcanic belt,
530   have suggested much larger amounts of recycled crust involved in the generation of both mafic and
531   intermediate arc magmas; from >60% in conjunction with diapiric uprise and melting of subducted
532   crust [58] to 100% resulting in the generation of andesites by bulk melting of subducted crust
533   "relaminated" below the mantle wedge [63].

534   *5.2. El Teniente deposit*

535   The giant El Teniente Cu-Mo deposit originally contained ≥100 million metric tonnes (Mt) of Cu
536   [32,33]. Pb, S and Os isotopic data [43-45,65] indicate that Cu, Mo and S were derived from the
537   associated igneous rocks. O and H isotopic and fluid inclusion data suggest that these metals were
538   transported and deposited by high-temperature magmatic fluids [38,39,66], and a significant
539   proportion of the Cu ore is contained with magmatic-hydrothermal breccia pipes [32-36]. Important
540   questions concerning the genesis of El Teniente, and any other giant orthomagmatic ore deposit, are:
541   1) Was the large amount of metal in the deposit derived from a large amount of magma or a unique
542   metal-rich magma?; and 2) How were the metals transferred from the magma into the host rocks?

543   Muñoz et al. [37] conclude that the high initial $\varepsilon_{Hf(t)}$ values (total average of +7.4) of the syn-
544   mineralization felsic plutons "rules out involvement of any significant crustal contamination in the
545   genesis of the El Teniente magmas." We agree, at least with regard to intra-crustal assimilation
546   (MASH). However, they then go on to suggest that, based "entirely on the near constant Hf isotopic
547   composition shown by the Cenozoic igneous of the region" they also "envision that Cenozoic
548   magmatism in central Chile originates from a MASH reservoir." We strongly disagree, given the clear
549   evidence that the $\varepsilon_{Hf(t)}$ values of Cenozoic magma, in particular mantle-derived mafic magmas
550   erupted in the region, were not at all constant, but progressively decreased significantly with time.

551   We suggest instead that the near constancy of the Hf isotopic composition of the 7.1 to 4.8 Ma
552   felsic plutons in the El Teniente deposit is a result of mixing, storage and homogenization (but not
553   crustal assimilation) of mantle-derived magmas in a large vertically zoned upper crustal magma
554   chamber (Figure 10) which developed as a result of compressive deformation after 7 Ma (Figure 8).
555   These mafic mantle-derived magmas provided heat, water, S and metals into the base of this magma
556   chamber [67], which became vertically stratified with more hydrous and more silica-rich magmas
557   closer to the surface. As the input of mantle-derived magmas decreased during the Late Miocene,
558   and uplift and erosion brought the roof of the chamber closer to the surface [12,13], the upper part of
559   the chamber crystallized and differentiated into the magmas that formed the felsic plutons. Although
560   the Hf isotopic composition of the mantle-derived magmas may have been evolving over this same
561   time period (Figure 7), the large volume of the magma chamber into which these magmas mixed
562   limited the variations observed within the progressively younger felsic plutons, although some small
563   decrease in their $\varepsilon_{Hf(t)}$ values is apparent. Once this large magma chamber fully crystallized, mantle-
564   derived olivine lamprophyre dikes were able to penetrate up to the surface, and these clearly exhibit
565   lower $\varepsilon_{Hf(t)}$ resulting from increased source region contamination of the mantle by subducted
566   components. Small barren plutons of the Young Plutonic Complex (5.5 to 6 Ma; Figure 5; [10]), which
567   occur outside the area of the deposit, also have more radiogenic characteristics than the felsic
568   porphyries of similar age within the deposit, presumably because they have not formed above such
569   a large, long-lived magma chamber and their isotopic compositions reflect more directly that of the
570   mantle-derived magmas that they were derived from. This is consistent with the suggestion that the
571   difference between barren plutons and the mineralized deposit reflects the size and longevity of the
572   magma chambers that lead to their formation.

573   Muñoz et al. [37] further suggest that, as a result of crustal thickening, dehydration melting in
574   the deep crustal hot zone [68] within which the MASH reservoir was located "probably influenced
575   the fertility of the magmas by increasing the melt component derived from this process relative to
576   the component derived from primary" mantle melts. They do not detail what specific characteristics

577   make a magma more "fertile", but they note that dehydration melting leads to the development of
578   water undersaturated magmas, which are less, not more likely to be able to exsolve mineral-rich
579   magmatic fluids.
580   In contrast, we conclude that the mantle-derived olivine basalts emplaced in the Teniente Mafic
581   Complex prior to the development of the large magma chamber below the deposit, and the mantle-
582   derived olivine lamprophyres which cut through the deposit after this magma chamber fully
583   solidified, have changed their isotopic compositions due to increased contamination of the mantle
584   source region with subducted components, but we do not observe [22,23] any significant change in
585   the Cu contents between the pre-mineralization olivine basalts (100 ppm) and the post-mineralization
586   olivine lamprophyres (100 ppm). Therefore we do not believe that source region contamination
587   generated a uniquely "fertile" magma with respect to Cu content. We have suggested instead that
588   the large amount of Cu in the deposit reflects a large amount of magma in the chamber above which
589   the deposit developed [38,39,69,70]. To produce the $\geq 100 \times 10^6$ tonnes of Cu in the deposit requires a
590   batholith-size (≥ 600 km^3) amount of magma with ~100 ppm Cu. What made the deposit giant was
591   that over the ~3 m.y. period that a magma chamber existed below the developing deposit, Cu, S heat
592   and water from mantle derived magmas were added continuously to the base of the chamber and
593   subsequently concentrated near the roof of the chamber by volatile transport. Clearly, because of
594   increased source region contamination by subducted materials the mantle wedge did also became
595   progressively more hydrated, ultimately leading to the generation of lamprophyric magmas, which
596   require 6-16 wt % H$_2$O, instead of olivine basalts, which require only 2 wt % H$_2$O [52-55]. Increasing
597   H$_2$O content of the mantle-derived magmas through the time that they were mixed into the overlying
598   magmas chamber may have resulted in more oxidizing conditions within the chamber, enhancing
599   the process of volatile transfer of S and metals towards the roof of the chamber (Figure 10; [49,51,71]).

600
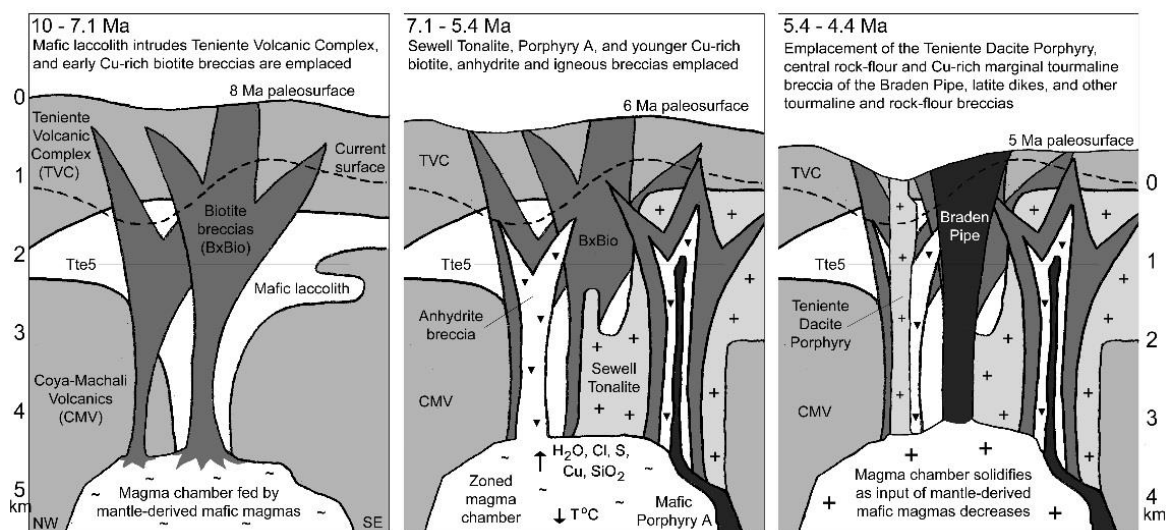
601   **Figure 10.** Model for the multistage development of the El Teniente deposit [23,32,33,39]. The main
602   features of the model include (1) a large, long-lived (≥ 3 Myr) open-system magma chamber,
603   crystallizing at ≥ 4 km depth, fed from below by mantle-derived mafic magmas and exsolving mineral-
604   rich high-temperature magmatic fluids through its roof to produce the large breccia pipes that are
605   prominent features this deposit; (2) decreasing magma supply in the Late Miocene and Pliocene as
606   subduction angle decreases, leading to crystallization and solidification of this chamber; (3)
607   progressive uplift and erosion that enhances this crystallization and solidification process and results
608   in telescoping of different types of breccia and igneous rocks [12,13]; (4) progressive igneous
609   differentiation of the magma chamber associated with crystallization and volatile loss, generating
610   felsic porphyries that intrude previously mineralized rocks above the chamber. No coeval volcanism
611   is known to have occurred during mineralization, but once the chamber solidified, post-
612   mineralization mantle-derived olivine lamprophyre dikes were emplaced. (Reprinted from Journal of
613   Petrography, volume 52, C.R. Stern et al., Magmatic evolution of the giant El Teniente Cu-Mo deposit,
614   central Chile, page 1607, Copyright 2011, with permission from Oxford University Press.)

Older studies of El Teniente suggested that Cu was transferred into the host rocks in association with the intrusion of the Teniente Dacite Porphyry, but new age dates indicate that much of the mineralization precedes this event, and that where this essentially barren porphyry intrudes outside the deposit, it creates only alteration but not mineralization. Instead we have suggested that the Cu and S were transferred into the host rocks of the deposit from the roof of the large magma chamber by exsolution of high-temperature metal-rich fluids generating multiple large magmatic-hydrothermal mineralized breccia complexes such as the central Braden Pipe, and El Teniente is thus better classified as a megabreccia deposit (Figure 10; [23,32,33,38,39]. Vry et al. [36] proposed that such breccias formed in association with the intrusion of the small dacite and diorite dikes to the northeast of the Braden pipe (Figure 6). However, we suggest instead that the breccias formed first and the porphyries intruded into the zone of weakness created by the breccias, since some of these porphyry bodies, such as Porphyry A (Figure 6) contain clasts of the breccias they intrude, and others of these small porphyries have no associated breccias surrounding them.

6. Conclusions

The Hf isotopic data are consistent with the Sr, Nd and Pb data, and imply the incorporation of small, but progressively increasing proportions of continental crust into the mantle source of the mafic magmas erupted in the vicinity of El Teniente between ≥15 and 2.3 Ma.

The felsic plutons in the deposit formed by mixing, storage and homogenization, combined with crystal-liquid differentiation, but not crustal assimilation (not MASH), in a large, long-lived, vertically zoned magma chamber that developed due to compressive deformation and persisted between the period ~7 to 4.6 Ma.

Progressively more hydrous and radiogenic mantle-derived mafic magmas feed this chamber from below, providing heat, H_2O, S and metals, but no unique "fertile" Cu-rich magma was involved in the formation of the deposit.

As the volume of these mantle-derived magmas decreased from the Late Miocene into the Pliocene, the chamber crystallized and solidified, producing both felsic plutons and large magmatic-hydrothermal breccias that emplaced Cu and S into the older (≥8.9 Ma) mafic Teniente Mafic Complex host rocks of the deposit. The deposit is therefore best classified as a megabreccia deposit.

Author Contributions: Conceptualization, Charles R Stern, M Alexandra Skewes and Alejandra Arévalo; Data curation, Kwan-Nang Pang and Hao-Yang Lee; Project administration, Charles R Stern, M Alexandra Skewes and Alejandra Arévalo; Writing – original draft, Charles R Stern; Writing – review and editing, Kwan-Nang Pang, Hao-Yang Lee, M Alexandra Skewes and Alejandra Arévalo.

Funding: The analytical work was supported by Ministry of Science and Technology, Republic of China (Taiwan) grant MOST 105-2628-M-001-002-MY4 to K.-N.P.

Acknowledgments: We thank Patricio Zuñiga, Ricardo Floody, Domingo Espiñeira and René Padilla for collaboration in the collection and characterization of the samples from El Teniente, and two reviewers for their constructive comments.

Conflicts of Interest: We have no conflicts of interests.

References

1. Hickey-Vargas, R. Peeled or MASHed? *Nature* **1991**, *350*, 381-382.

2. Hildreth, W.; Moorbath, S. Crustal contributions to arc magmatism in the Andes of central Chile. *Contrib. Mineral. Petrol.* **1988**, *103*, 361-386.

3. Stern, C.R. Role of subduction erosion in the generation of Andean magmas. *Geology* **1991**, *19*, 78-81.

4. Stern, C.R. Active Andean volcanism: its geologic and tectonic setting. *Rev. Geol. Chile* **2004**, *31*, 161-208.

659   5.   Stern, C.R. Subduction erosion: rates, mechanisms, and its role in arc magmatism and the evolution of the
660   continental crust and mantle. *Gondwana Res.* **2011**, *20*, 284–308.

661   6.   Rutland, R.W.R. Andean orogeny and ocean floor spreading. *Nature* **1971**, *233*, 252-255.

662   7.   Goss, A.R.; Mahlburg Kay, S.; Mpodozis, C. Andean adakite-like high-Mg andesites on the Northern
663   margin of the Chilean-Pampean flat-slab (27–28.5°S) associated with frontal arc migration and fore-arc
664   subduction erosion. *J. Petrol.* **2013**, *54*, 2193–2234.

665   8.   Risse, A.; Trumbull, R.B.; Kay, S.M.; Coira, B.; Romer, R.L. Multi-stage evolution of Late Neogene mantle-
666   derived Magmas from the Central Andes Back-arc in the Southern Puna Plateau of Argentina. *J. Petrol.*
667   **2013**, *10*, 1963–1995.

668   9.   Lamb. S.; Davis, P. Cenozoic climate change as a possible cause for the rise of the Andes. *Nature* **2003**, *425*,
669   792-797.

670   10.   Kay, S.M.; Godoy, E.; Kurtz, A. Episodic arc migration, crustal thickening, subduction erosion, and
671   magmatism in the south-central Andes. *Geol. Soc. Amer. Bull.* **2005**, *117*, 67-88.

672   11.   Holm, P.M.; Søager, N.; Thorup-Dyhr, C.; Rohde-Nielsen, M. Enrichments of the mantle sources beneath
673   the Southern Volcanic Zone (Andes) by fluids and melts derived from abraded upper continental crust.
674   *Contrib. Mineral. Petrol.* **2014**, *167*, 1004.

675   12.   Skewes, M.A.; Holmgren, C. Solevantamiento Andino, erosión y emplazamiento de brechas mineralizadas
676   en el depósito de cobre porfídico Los Bronces, Chile Central (33°S): aplicación de termometría de
677   inclusiones fluidas. *Rev. Geol. Chile* **1993**, *20*, 71-84.

678   13.   Skewes, M.A.; Stern, C.R. Tectonic trigger for the formation of late Miocene Cu-rich breccia pipes in the
679   Andes of central Chile. *Geology* **1994**, *22*, 551-554.

680   14.   Kurtz, A.C.; Kay, S.M.; Charrier, R.; Farrar, E. Geochronology of Miocene plutons and exhumation history
681   of the El Teniente region, Central Chile (34-35°S). *Rev. Geol. Chile* **1997**, *16*, 145-162.

682   15.   Charrier, R.; Baeza, O.; Elgueta, S.; Flynn, J.J.; Gans, P.; Kay, S.M.; Muñoz, N.; Wyss, A.R.; Zurita, E.
683   Evidence for Cenozoic extensional basin development and tectonic inversion south of the flat-slab segment,
684   southern Central Andes, Chile (33°-36°S.L.). *J. S. Amer. Earth Sci.* **2002**, *15*, 117-139.

685   16.   Giambiagi, L.B.; Ramos, V.A. Structural evolution of the Andes in a transitional zone between flat and
686   normal subduction (33°30-33°45'S), Argentina and Chile. *J. S. Amer. Earth Sci.* **2002**, *15*, 101-116.

687   17.   Nyström, J.; Vergara, M.; Morata, D.; Levi, B. Tertiary volcanism during extension in the Andean foothills
688   of central Chile (33°15'-33°45'S). *Geol. Soc. Amer. Bull.* **2003**, *115*, 1523-1537.

689   18.   Farías, M.; Charrier, R.; Carretier, S.; Martinod, J.; Fock, A.; Campbell, D.; Cáceres, J.; Comte, D. Late
690   Miocene high and rapid surface uplift and its erosional response in the Ande of central Chile (33º-35ºS).
691   *Tectonics* **2008**, *27*, TC1005.

692   19.   Farías, M.; Comte, D.; Charrier, R.; Martinod, J.; Tassara, A.; Fock, A. Crustal-scale structural architecture
693   of the central Chile Andes based on 3D seismic tomography, seismicity, and surface geology: implications
694   for mountain building in subduction zones. *Tectonics* **2010**, *29*, TC3006.

695   20.   Giambiagi, L.B.; Mescua, J.; Bechis, F.; Tassara, A.; Hoke, G. Thrust belts of the southern Central Andes:
696   Along-strike variations in shortening, topography, crustal geometry, and denudation: *Geol. Soc. Amer. Bull.*
697   **2012**, *124*, 1339–1351.

698   21.   Stern, C.R.; Skewes, M.A. Miocene to present magmatic evolution at the northern end of the Andean
699   Southern Volcanic Zone, central Chile. *Rev. Geol. Chile* **1995**, *22*, 261-272.

700   22.   Stern, C.R.; Floody, R.; Espiñeira, D. Pliocene olivine-hornblende-lamprophyre dikes from Quebrada de
701   los Sapos, El Teniente, Central Chile (34°S): Implications for the subarc mantle. *Andean Geol.* **2011**, *38*, 1-22.

23. Stern, C.R.; Skewes, M.A.; Arévalo, A. Magmatic evolution of the giant El Teniente Cu-Mo deposit, Central Chile. *J. Petrol.* **2012**, *52*, 1591-1617.

24. Muñoz, M.; Farías, M.; Charrier, R.; Fanning, C.M.; Polvé, M.; Deckart, K. Isotopic shifts in the Cenozoic Andean arc of central Chile: records of an evolving basement throughout cordilleran arc mountain building. *Geology* **2013**, *41*, 931-934.

25. Stern, C.R. Pliocene to present migration of the volcanic front, Andean Southern Volcanic Zone. *Rev. Geol. Chile* **1989**, *16*, 145-162.

26. Yáñez, G.; Ranero, C.; von Huene, R.; Díaz, J. Magnetic anomaly interpretation across the southern Central Andes (32°-33.5°S): the role of the Juan Fernández ridge in the late Tertiary evolution of the margin. *J. Geophys. Res.* **2001**, *106*, 6325-6345.

27. Yáñez, G.; Cembrano, J.; Pardo, M.; Ranero, C.; Selles, D. The Challenger-Juan Fernández-Maipo major tectonic transition of the Nazca-Andean subduction system at 33-34°S: geodynamic evidence and implications. *J. S. Amer. Earth Sci.* **2002**, *15*, 23-38.

28. Lindgren, W.; Bastin, E.S. Geology of the Braden mine, Rancagua, Chile. *Econ. Geol.* **1922**, *17*, 75-99.

29. Howell, F.H.; Molloy, S. Geology of the Braden orebody, Chile, South America. *Econ. Geol.* **1960**, *70*, 863-905.

30. Camus, F. Geology of the El Teniente orebody with emphasis on wall-rock alteration. *Econ. Geol.* **1975**, *70*, 1341-1372.

31. Cuadra, P. Geocronología K-Ar del yacimiento El Teniente y áreas adyacentes. *Rev. Geol. Chile* **1986**, *27*, 3-26.

32. Skewes, M.A.; Arévalo, A., Floody, R., Zuñiga, P.; Stern, C.R. The giant El Teniente breccia deposit: hypogene copper distribution and emplacement. In *Global Exploration 2002: Integrated Methods of Discovery*, Goldfarb, R.J., Nielson, R.L. Eds.; Society of Economic Geologists: USA, 2002; Special Publications 9, pp. 299-332.

33. Skewes, M.A.; Arévalo, A.; Floody, R.; Zuñiga, P.; Stern, C.R. The El Teniente megabreccia deposit, the world's largest copper deposit. In *Super Porphyry Copper and Gold Deposits: A Global Perspective*, Porter, T.M., Ed.; PGC Publishing: Adelaide, Australia, 2005; Volume 1, pp. 83-114.

34. Maksaev, V.; Munizaga, F.; McWilliams, M.; Fanning, M.; Marther, R.; Ruiz, J.; Zentilli, M. Chronology for El Teniente, Chilean Andes, from U-Pb, $^{40}Ar/^{39}Ar$, Re-Os, and fission track dating: implications for the formation of a supergiant porphyry Cu-Mo deposit. In *Andean Metallogeny: New Discoveries, Concepts and Updates*, Sillitoe, R.H., Perelló, J., Vidal, C.E. Eds.; Society of Economic Geologists: USA, 2004; Special Publications 11, pp. 15-54.

35. Cannell, J.; Cooke, D.; Walshe, J.L.; Stein, H. Geology, mineralization, alteration, and structural evolution of El Teniente porphyry Cu-Mo deposit. *Econ. Geol.* **2005**, *100*, 979-1004.

36. Vry, V.H.; Wilkinson, J.J.; Seguel, J.; Millán, J. Multistage intrusion brecciation and veining at El Teniente, Chile: evolution of a nested porphyry system. *Econ. Geol.* **2010**, *105*, 119-153.

37. Muñoz, M.; Charrier, R.; Fanning, C.M.; Maksaev, V.; and Deckart, K. Zircon trace element and O-Hf isotope analyses of mineralized intrusions from El Teniente ore deposit, Chilean Andes: Constraints on the source and magmatic evolution of porphyry Cu-Mo related magmas. *J. Petrol.* **2012**, 53, 1091–1122.

38. Skewes, M.A.; Stern, C.R. Genesis of the giant Late Miocene to Pliocene copper deposits of central Chile in the context of Andean magmatic and tectonic evolution. *Internat. Geol. Rev.* **1995**, *37*, 71-84.

39. Stern, C.R.; Skewes, M.A. Origin of giant Miocene and Pliocene Cu-Mo deposits in Central Chile: Role of ridge subduction, decreased subduction angle, subduction erosion, crustal thickening and long-lived,

batholiths-size, open system magma chambers. In *Super Porphyry Copper and Gold Deposits: A Global Perspective,* Porter, T.M., Ed.; PGC Publishing: Adelaide, Australia, 2005; Volume 1, pp. 65-82.

40. Warnaars, F.W.; Holmgren, C; Barassi, S. Porphyry copper and Tourmaline breccias at Los Bronces-Río Blanco, Chile. *Econ. Geol.* **1985**, *80*, 1544-1565.

41. Skewes, M.A.; Stern, C.R. Late Miocene mineralized breccias in the Andes of central Chile: Sr- and Nd-isotopic evidence for multiple magmatic sources. In Andean Copper Deposits,   Camus, F., Sillitoe, R.H., Petersen, R., Eds.; Society of Economic Geologists: USA, 1996; Special Publications 5, pp. 119-130.

42. Skewes, M.A.; Holmgren, C.; Stern, C.R. The Donoso copper-rich, tourmaline-bearing breccia pipe in central Chile: petrologic, fluid inclusion and stable isotope evidence for an origin from magmatic fluids. *Mineral. Deposita* **2003**, *38*, 2-21.

43. Kusakabe, M.; Hori, M.; Nakagawa, S.; Matsuhisa, Y.; Ojeda, J.M.; Serrano, L.M. Oxygen and sulfur isotopic compositions of quartz, anhydrite and sulfide minerals from the El Teniente and Río Blanco porphyry copper deposits, Chile. *Bull. Geol. Survey Japan* **1984**, *35*, 583-614.

44. Kusakabe, M., Hori, M. & Matsuhisa, Y.   Primary mineralization-alteration of the El Teniente and Río Blanco porphyry copper deposits, Chile; stable isotope, fluid inclusion and Mg+2/Fe+2/Fe+3 ratios of hydrothermal fluids. In *Stable Isotopes and Fluid Processes in Mineralization*, Herbert, H.K., Ho, S.E., Eds.; University of Western Australia Press, Perth, Australia, 1990; pp. 244-259.

45. Puig, A. Geologic and metallogenic significance of the isotopic composition of lead in galenas of the Chilean Andes. *Econ. Geol.* **1988**, *83*, 843-858.

46. Muñoz, M.; Fuentes, F.; Vergara, M.; Aguirre, L.; Nyström, J.O. Abanico East Formation: petrology and geochemistry of volcanic rocks behind the Cenozoic arc front in the Andean Cordillera, central Chile (33°50'S). *Rev. Geol. Chile* **2006**, *33*, 109-140.

47. Montecinos, P.; Schárer, U.; Vergara, M.; Aguirre, L. Lithospheric origin of Oligocene--Miocene magmatism in Central Chile: U-Pb ages and Sr-Pb-Hf isotope composition of minerals. *J. Petrol*. **2008**, *49*, 555-580.

48. Godoy, E.; Yáñez, G.; Vera, E. Inversion of an Oligocene volcanic^ tectonic basin and uplifting of its superimposed Miocene magmatic arc in the Chilean Central Andes: first seismic and gravity evidences. *Tectonophys*. **1999**, *306*, 217-236.

49. Stern, C.R.; Funk, J.A.; Skewes, M.A.; Arévalo, A. Magmatic anhydrite in plutonic rocks at the El Teniente C^Mo deposit, Chile, and the role of sulfur- and copper-rich magmas in its formation. *Econ. Geol.* **2007**, *102*, 1335-1344.

50. Deckart, K.; Godoy, E.; Bertens, A.; Saeed, A.; Jeréz, D. Barren Miocene granitoids in the central Andean metallogenic belt, Chile: Geochemistry and Nd-Hf and U-Pb isotope systematics: *Andean Geol.* **2010**, *37*, 1–31.

51. Blatter, D.K.; Carmichael, I.S.E. Hornblende peridotite xenoliths from central Mexico reveal the highly oxidized nature of subarc upper mantle. *Geology* **1998**, *26*, 1035-1038.

52. Blatter, D.K.; Carmichael, I.S.E. Hydrous phase equilibria of a Mexican high-silica andesite: a candidate for mantle origin? *Geochim. Cosmochim. Acta* **2001**, *65*, 4043-4065.

53. Moore, G.M.; Carmichael, I.S.E. The hydrous phase equilibra (to 3kbar) of an andesite and basaltic andesite from Western Mexico: constraints on water content and conditions of phenocrysts growth. *Contrib. Mineral. Petrol.* **1998**, *130*, 304-319.

54. Carmichael, I.S.E. The andesite aqueduct: perspectives in the evolution of intermediate magmas in west-central Mexico. *Contrib. Mineral. Petrol.* **2002**, *143*, 641-663.

55. Barcley, J.; Carmichael, I.S.E. A Hornblende Basalt from Western Mexico: Water-saturated Phase Relations Constrain a Pressure-Temperature Window of Eruptibility. *J. Petrol.* **2004**, *45*, 485-506.

56. Rudnick R.; Gao S. Composition of the continental crust. In *The Crust*, R. L. Rudnick, R.L., Ed.; Elsevier-Pergamon, Oxford, Englanf, 2002; pp. 1–64.

57. McDonough W.F.; Sun S.S. The composition of the Earth. *Chem. Geol.* **1995**, *120*, 223–253.

58. Straub, S.M.; Gómez-Tuena, A.; Bindeman, I.N.; Bolge, L.L.; Brandl, P.A.; Espinasa-Perena, R.; Solari, L.; Stuart, F.M.; Vannucchi, P.; Zellmer, G.F. Crustal recycling by subduction erosion in the central Mexican Volcanic Belt. *Geochim. Cosmochim. Acta* **2015**, *166*, 29–52.

59. Tera F.; Brown L.; Morris J.; Sacks I.S. Sediment incorporation in island-arc magmas: Inferences from [10]Be. *Geochim. Cosmochim. Acta* **1986**, *50*, 535–550.

60. Morris J.D.; Leeman W.P.; Tera F. The subducted component in island arc lavas: constraints from Be isotopes and B–Be systematics. *Nature* **1990**, *344*, 31–36.

61. Morris J.D.; Gosse J.; Brachfeld, S.; Tera F. Cosmogenic [10]Be and the solid earth: studies in geomagnetism, subduction zone processes, and active tectonics. In *Reviews in Mineralogy*, Grew, E., Ed.; Mineralogical Society of America, Washington, DC, USA, 2002; pp. 207–270.

62. Tonarini S.; Leeman W.P.; Leat P.T. Subduction erosion of forearc mantle wedge implicated in the genesis of the South Sandwich Island (SSI) arc: evidence from boron isotope systematics. *Earth Planet. Sci. Lett.* **2011**, *301*, 275–284.

63. Gómez-Tuena, A.; Cavazos-Tovar, J.G.; Parolari, M.; Straub, S.M.; Espinasa-Pereña, R. Geochronological and geochemical evidence of continental crust 'relamination' in the origin of intermediate arc magmas. *Lithos* **2018**, *322*, 52-66.

64. Goss, A.R.; Kay, S.M. Steep REE patterns and enriched Pb isotopes in southern Central American arc magmas: evidence for forearc subduction erosion? *Geochem. Geophys. Geosyst.* **2006**, *7*, 1-20.

65. Freydier, C.; Ruiz, J.; Chesley, J.; Candless, T.; Munizaga, F. Re-Os isotope systematics of sulfides from felsic igneous rocks: application to base metal porphyry mineralization in Chile. *Geology* **1997**, *25*, 775-778.

66. Klemm, L.M.; Pettke, T.; Heinrich, C.L.; Campos, E. Hydrothermal evolution of the El Teniente deposit, Chile: porphyry Cu-Mo ore deposition from low-salinity magmatic fluids. *Econ. Geol.* **2007**, *102*, 1021-1045.

67. Hattori, K.H.; Keith, J.D. Contributions of mafia melt for porphyry deposits: evidence from Pinatubo and Bingham. *Mineral. Deposita* **2001**, *36*, 799-806.

68. Annen, C.; Blundy, J.D.; Sparks, R.S.J. The genesis of intermediate and silica magmas in deep crustal hot zones. *J. Petrol.* **2006**, *47*, 505-539.

69. Cloos, M. Bubbling magma chambers, cupulas and porphyry copper deposits. *Internat. Geol. Revs.* **2001**, *43*, 285-311.

70. Richards, J.P. Cumulative factors in the generation of giant calc-alkaline porphyry Cu deposits. In *Super Porphyry Copper and Gold Deposits: A Global Perspective*, Porter, T.M., Ed.; PGC Publishing, Adelaide, Australia, 2005; Volume 1, pp. 7-26.

71. Garrido, I.; Cembrano, J.; Siña, A.; Stedman, P.; Yáñez, G.A. High magma oxidation state and bulk crustal shortening: key factors in the genesis of Andean porphyry copper deposits, central Chile (31-34°S). *Rev. Geol. Chile* **2002**, *29*, 43-54.